Journal of Advanced Ceramics
2021, **10**(4): 675–703
https://doi.org/10.1007/s40145-021-0500-3

ISSN 2226-4108
CN 10-1154/TQ

Review

Progress and perspectives in dielectric energy storage ceramics

Dongxu LI[a,b,†], Xiaojun ZENG[a,†], Zhipeng LI[a], Zong-Yang SHEN[a,*], Hua HAO[b], Wenqin LUO[a], Xingcai WANG[c], Fusheng SONG[a], Zhumei WANG[a], Yueming LI[a]

[a]*Energy Storage and Conversion Ceramic Materials Engineering Laboratory of Jiangxi Province, China National Light Industry Key Laboratory of Functional Ceramic Materials, School of Materials Science and Engineering, Jingdezhen Ceramic University, Jingdezhen 333403, China*
[b]*State Key Laboratory of Advanced Technology for Materials Synthesis and Processing, School of Materials Science and Engineering, Wuhan University of Technology, Wuhan 430070, China*
[c]*Chengdu Hongke Electronic Technology Co., Ltd., Chengdu 610000, China*

Received: February14, 2021; Revised: April 29, 2021; Accepted: May 17, 2021

Abstract: Dielectric ceramic capacitors, with the advantages of high power density, fast charge–discharge capability, excellent fatigue endurance, and good high temperature stability, have been acknowledged to be promising candidates for solid-state pulse power systems. This review investigates the energy storage performances of linear dielectric, relaxor ferroelectric, and antiferroelectric from the viewpoint of chemical modification, macro/microstructural design, and electrical property optimization. Research progress of ceramic bulks and films for Pb-based and/or Pb-free systems is summarized. Finally, we propose the perspectives on the development of energy storage ceramics for pulse power capacitors in the future.

Keywords: energy storage ceramics; dielectric; relaxor ferroelectric; antiferroelectric; pulse power capacitor

1 Introduction

Electric energy, as secondary energy, plays a dominant role in human daily life, industrial manufacture, and scientific research owing to its cost-effectiveness, versatility, and convenient transportation. Compared with traditional fossil fuels, electrical energy generated from renewable resources can effectively cope with resource depletion and reduce environmental pollution. However, the characteristics of intermittence, fluctuation, and randomness result in a time and space difference between practicality and expected demand, and thereby seriously hinder its large-scale development and application [1]. It is urgent to develop advanced technologies to address the issue of electric energy storage and conversion. Currently, the researches of energy storage technologies are mainly concentrated on dielectric capacitors [2,3], electrochemical capacitors [4], batteries [5], and solid oxide fuel cells [6], whose corresponding characteristics are given in Fig. 1.

Ceramic capacitor, as a passive component, possesses high power density (~GW/kg), fast charge–discharge speed (μs, or even ns), well fatigue endurance ($\geqslant 10^6$ cycles), and high temperature stability, playing an

† Dongxu Li and Xiaojun Zeng contributed equally to this work.
* Corresponding author.
E-mail: shenzongyang@163.com

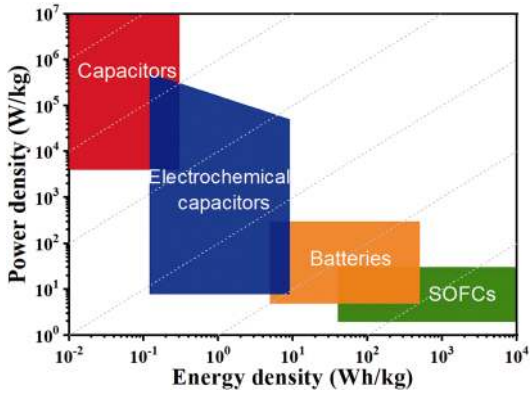

Fig. 1 Ragone pattern of different energy storage technologies.

indispensable role in solid-state power systems [1,7]. Generally, ceramic capacitors with a physical power supply based on dipole orientation, have relatively lower energy density than lithium-ion batteries and solid oxide fuel cells. Therefore, it is critical to improve the energy density of ceramic capacitors for expanding their practical applications.

Polarization behavior of dielectric materials under external electric field can be characterized by *P*–*E* loops (hysteresis loops) [8,9], as exhibited in Fig. 2. According to different *P*–*E* loop characteristics, dielectric materials can be classified into linear dielectric, ferroelectric, and antiferroelectric, of which ferroelectric includes normal ferroelectric and relaxor ferroelectric. Based on basic principle and reported literature, the polarization of linear dielectric is linearly proportional to the electric field, whereas its relatively low dielectric constant (ε_r) makes it difficult to achieve high energy density. Normal ferroelectric also possesses limited energy density because of its high remanent polarization (P_r). Relaxor ferroelectric and antiferroelectric could achieve both high energy density and efficiency, owing to their relatively high maximum polarization (P_{max}), low remanent polarization (P_r), and moderate breakdown strength (E_b), and thus have been considered to be the most potential candidates for pulse power systems.

Currently, the researches of energy storage ceramics are mainly concentrated on bulk (> 100 μm), thick film (1–100 μm), and thin film (< 1 μm). It should be noted that these three dielectric ceramics categories possess a big difference in actual energy storage capability, and thus one cannot treat them as one object in the same way. Meanwhile, the device application type also has different categories: ceramic bulk, multilayer structure capacitor, flexible electronic, integrated circuit, etc. This review combines the related work of authors, discusses the progress of energy storage performances of linear dielectric, relaxor ferroelectric, and antiferroelectric with emphasis on composition modification, macro/microstructural modulation, and electrical property optimization.

2 Key parameters for evaluating energy storage properties

2. 1 Energy storage density

Generally, energy storage density is defined as energy in per unit volume (J/cm^3), which is calculated by [2]:

$$W = \int_0^{D_{max}} E\mathrm{d}D \tag{1}$$

where W, E, D_{max}, and dD are the total energy density, applied electric field, maximum electric displacement at E, and increment of electric displacement per unit of the electric field, respectively. For ceramic dielectric, D is an unmeasurable microscopic physical quantity, and is usually expressed by polarization as following:

$$D = \varepsilon_0 E + P \tag{2}$$

Meanwhile, P is dependent on E as follows:

$$P = \varepsilon_0 \chi E \tag{3}$$

where ε_0 is the vacuum dielectric constant of 8.854 × 10^{-12} F/m, χ is the dielectric polarization coefficient, so

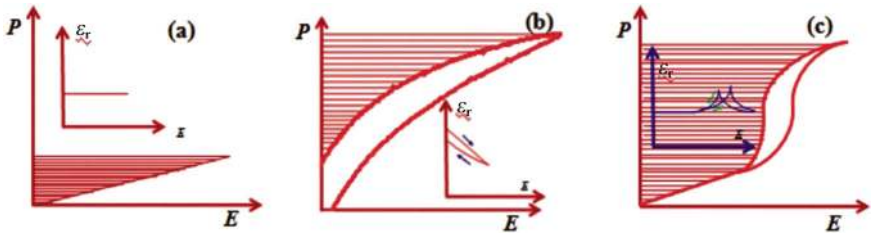

Fig. 2 Typical dependence of polarization and permittivity on electric field for (a) linear dielectric, (b) relaxor ferroelectric, and (c) antiferroelectric. Reproduced with permission from Ref. [2], © WILEY-VCH Verlag GmbH & Co. KGaA, Weinheim 2017.

that Eq. (2) can be expressed as

$$D = \varepsilon_0(\chi + 1)E = \varepsilon_0\varepsilon_r(E)E \quad (4)$$

where $\varepsilon_r(E)$ is the relative dielectric constant at E. Therefore, Eq. (1) after the change is as follows:

$$W = \int_0^{E_{max}} \varepsilon_0\varepsilon_r(E)E\mathrm{d}E \quad (5)$$

It is obvious that high ε_r and high E_b are important factors for achieving high W [10]. However, these two factors are hard to obtain simultaneously in a given material due to the trade-off relationship.

It should be noted that W is a sum of effective energy density (W_{rec}) and energy loss (W_{loss}) [8,11]. In practice, W_{rec} is more important than W in evaluating the energy storage performances of dielectric materials. As shown in Fig. 2, W_{rec} is determined by the area enclosed by the discharge curve of its P–E loops and the polarization axis. The equation is given as follows:

$$W_{rec} = \int_{P_r}^{P_{max}} E\mathrm{d}P \quad (6)$$

Obviously, high P_{max}, low P_r (i.e., large $\Delta P = P_{max}–P_r$), and high E_b are essential factors to achieve high W_{rec}.

2. 2 Energy storage efficiency

Energy storage efficiency (η) is another important parameter to evaluate energy storage performances of dielectric materials, which is expressed as

$$\eta = \frac{W_{rec}}{W} \times 100\% = \frac{W_{rec}}{W_{rec} + W_{loss}} \times 100\% \quad (7)$$

where W_{loss} is the energy loss during the discharge process, which equals to the area enclosed by the P–E loop in number. W_{loss} is mainly dissipated as heat, and a higher value means a stronger negative effect on the service life of ceramic capacitors. Therefore, it is vital that P–E loops gradually go slim to enhance η, and then improve its practical application.

According to Eqs. (6) and (7), P–E loops go slim accompanied with high P_{max}, low P_r (i.e., high $\Delta P = P_{max}–P_r$), and high E_b, which become the key issues in optimizing the energy storage characteristics of dielectric materials. There are two strategies: For one, to optimize the polarization behavior and strengthen their relaxor characteristics, which means that P–E loops go slim; for the other, to improve the breakdown behavior of dielectric ceramics, i.e., enhancing its E_b. This paper chooses linear dielectric, relaxor ferroelectric, and antiferroelectric as targets, and discusses the influences of chemical modification and macro/microstructural design on polarization behavior and breakdown strength of dielectric materials.

2. 3 Rapid charging–discharging characteristics

Generally, energy storage performances of ceramic materials can be reflected by P–E loops measured by a modified Sawyer–Tower circuit. Meanwhile, the energy storage characteristics of ceramic capacitors, including effective discharging time ($t_{0.9}$) and power density (P), are more accurately reflected by the charging–discharging curve recorded at a specific RLC circuit [12]. The simple equivalent circuit model is exhibited in Fig. 3(a). In the charging process ("1" connected to "3"), the potential difference (Φ) between two surfaces of capacitor equals the applied voltage (V), representing the charging process is finished. And then, the vacuum switches automatically and quickly rotate ("2" connected to "3") to achieve the discharging process. Current flows to the oscilloscope via a load (R_0), which is recorded as wave function as a function of time. The discharging density is given by

$$J(t) = \frac{\int_0^t V(t)I(t)\mathrm{d}t}{\varphi} = \frac{\tau V_0^2}{2\varphi R_0}\left(1 - \mathrm{e}^{-\frac{2t}{\tau}}\right) \quad (8)$$

where φ is the effective volume, τ is the relaxation time, and $V(t)$ and $I(t)$ are the voltage and current as function of time, respectively. Discharging current (I) and energy density (J) versus time (t) are shown in Fig. 3(b).

It is reported that the value of J calculated by Eq. (8) is generally smaller than that of W_{rec}. For the reasons, it may be closely related to two factors. Firstly, the domains cannot switch and orientate promptly due to fast discharge speed, and thus the energy is not completely released [13]. Secondly, the circuit has equivalent series resistance that generates Joule energy [14]. In order to acquire higher value of J and W_{rec}, reducing domain size (e.g., polar nanoregions) only from material itself may be an effective method [15].

Power density (P) is also an important parameter of dielectric ceramic capacitors, which is determined as follows:

$$P = \frac{\pi f \varepsilon_0\varepsilon_r E_b^2}{2\tan\delta} \quad (9)$$

where f is the testing frequency, and the others are the same as those discussed above. It can be seen that high ε_r, high E_b, and low $\tan\delta$ are the basic requirements of

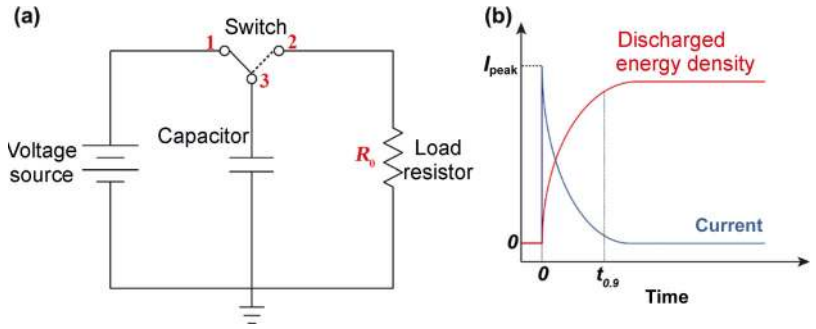

Fig. 3 (a) Circuit of charging–discharging. (b) Discharging current (I) and energy density (J) versus time. Reproduced with permission from Ref. [1], © Elsevier Ltd. 2018.

achieving high P. Meanwhile, P has an obvious dependence on frequency (f), which means high f corresponds to high P. In addition, $t_{0.9}$ is an important factor for influencing the practical application of ceramic capacitors. The smaller the value of $t_{0.9}$, the stronger the pulse current can be generated in a short time. It is worth mentioning that the value of $t_{0.9}$ is dependent on not only the intrinsic properties of the dielectric materials, but also some external factors. For example, Li *et al.* [15] found that $t_{0.9}$ can be controlled by adjusting the load (R_0) in the circuit.

2. 4 Reliability of work

No matter with dielectric material or pulse capacitor, the reliability of work is a crucial factor to influence its application scenes. Generally, reliability of work requires keeping stability of electric properties of material and device under thermal, electric, mechanical, magnetic, etc., external field stimulus.

Temperature stability usually requires that dielectric properties and polarization of material have a gentle fluctuation as a function of temperature. For example, dielectric constant needs to maintain a ±15% variation over a temperature range from −55 to 125 ℃ (X7R), to 150 ℃ (X8R), and even to 300 ℃, especially in high temperature working environments. Therefore, one should know the Joule heat categories: dielectric loss or leakage current, and to solve corresponding issues. Generally, different electric field conditions such as cycle number, frequency, voltage category, magnitude, etc., all require keeping good energy storage stability. Specially, fatigue endurance is a very important issue to influence capacitor working capability. In 2009, Lou [16] reviewed different fatigue mechanisms in ceramic bulks, films, and single crystalline, which help us better understand fatigue behavior of material. In addition, mechanic and magnetic fields both influnence its polarization behavior of material, and its importance may be playing a crucial role in the future multi-functional coupling requirement. Therefore, the evaluation criterion of reliability of working should be a complicated project.

3 Dielectric ceramics for energy storage capacitors

As given in Fig. 2, dielectric materials mainly include three categories, namely linear dielectric, relaxor ferroelectric, and antiferroelectric. Therefore, we here compare and analyze the energy storage properties of some representative dielectric ceramic bulks and films.

3. 1 Linear dielectric ceramics

Linear dielectric ceramics usually possess characteristics of low ε_r and tanδ, as well as moderate E_b. It is thereby hard to obtain high W_{rec} despite under high electric field. In this regard, the researches of linear dielectric ceramics are mainly concentrated on increasing ε_r or improving polarization behavior based on maintaining high E_b.

3.1.1 TiO_2 based ceramics

TiO_2 is a typical linear dielectric, with characteristics of moderate E_b (> 350 kV/cm), low tanδ (< 0.1%), dielectric constant (~110), and wide band gap (~3.2 eV), and thus receives wide use in contemporary electronic ceramic industries and photocatalysis field [17–20]. Generally, TiO_2 has three crystal structures including orthorhombic brookite, tetragonal rutile, and anatase. The rutile phase is more stable and easier to be synthesized than others, and hence gains more attention in ceramic bulks and films [21,22].

In 2013, Hu *et al.* [23] firstly reported that (In, Nb)

co-doped TiO_2 ceramics displayed a giant dielectric constant ($> 10^4$) as well as low tanδ ($< 5\%$), and possessed good temperature and frequency stabilities over a wide temperature range (80–450 K). The authors claim that this phenomenon should be closely related to defect clusters and localized electrons, and thus propose a "localized defect polarization" mechanism. However, the specified reason of giant dielectric constant appearing in donor/acceptor co-doped TiO_2 ceramics still has some controversies. Li *et al.* [24,25] attempted to explain the phenomenon by using an internal barrier layer capacitance (IBLC) model, similar to $CaCu_3Ti_4O_{12}$ (CCTO) ceramics from extrinsic factors influencing dielectric constant. Actually, most of subsequent discussion on the physical origin of different-type donor/acceptor co-doped TiO_2 ceramics is basically around above two mechanisms [26–28], even though no significant progress has been achieved in W_{rec} for donor/acceptor co-doping TiO_2 ceramics because of the expense of a rapid reduction in E_b.

In another way, improving the sintering behavior of TiO_2-based ceramics would be effectively enhancing E_b, such as refining grain size [17,29], adding glass phase [30], applying special sintering technology (SPS), and so on. Liu *et al.* obtained a W_{rec} of 1.15 J/cm^3 for alkali-free glass modified TiO_2 ceramics at 501.7 kV/cm. Unfortunately, W_{rec} of those ceramic bulks after different modification ways is still only at a scale of 1 J/cm^3, which is less than other energy storage dielectric materials. It should be noticed that high quality TiO_2 film is a good direction owing to their high E_b. For instance, Chao and Dogan [31] fabricated 0.1-mm thick TiO_2 films using tape-casting method, which achieve W_{rec} of 14 J/cm^3 at 1400 kV/cm.

3.1.2 *$SrTiO_3$ based ceramics*

$SrTiO_3$ (ST) is a cubic paraelectric phase with ABO_3 type perovskite structure, accompanying to space group of $Pm\bar{3}m$ and lattice constant of a = 3.905 Å [32,33]. ST ceramics possess moderate ε_r of ~300, E_b of ~100 kV/cm, and low tanδ of ~10^{-3}, as well as good temperature-, frequency-independent dielectric properties, bias voltage stability, and thermoelectric energy conversion efficiency [34–36]. Therefore, it is considered to be a potential energy storage and conversion candidate. Compared with TiO_2 ceramic (~110) and polymer linear dielectric (< 10), ST has an advantage of relatively high ε_r, and thus is more suitable for pulse capacitor.

Utilizing Ca^{2+}, Ba^{2+}, and Pb^{2+} ions to replace Sr^{2+} on the A-site of ST could adjust the Curie temperature (T_C) to room temperature, and thus dielectric constant could be enhanced [37,38]. Especially, $Ba_xSr_{1-x}TiO_3$ (BST) solid solutions combine the characteristics of high E_b of $SrTiO_3$ and high ε_r of $BaTiO_3$, and receive much more attention in recent years [39]. The structure and performance of BST can be adjusted over a wide range to meet the requirements of different applications. As the molar fraction of Ba increases from 0 to 1, phase composition of BST varies from cubic paraelectric (ST) to tetragonal ferroelectric (BT), accompanying by the T_C increase from near absolute 0 to ~393 K. According to theoretical calculation of BST solid solution by Fletcher *et al.* [40], it is easier to obtain an ideal energy storage property if the T_C of the ceramic composition is far away the working temperature. Thereby, BST compositions with $x \leqslant 0.4$ would be more suitable pulse power capacitor candidates because *P*–*E* loops display linear or weak nonlinear characteristic at room temperature, as shown in Fig. 4. In 2015, Wang *et al.* [37] investigated energy storage performances of $Ba_xSr_{1-x}TiO_3$ ($x \leqslant 0.4$) ceramics, and found that $Ba_{0.4}Sr_{0.6}TiO_3$ achieved the highest W_{rec}, while relatively low and rapidly decreased η becomes a serious problem to hinder its application. By comparison, $Ba_{0.3}Sr_{0.7}TiO_3$ possessed moderate W_{rec}, high η ($\geqslant 95\%$), and very low dielectric loss (tanδ = 7.6×10^{-4} @ 1 kHz), making it more suitable for the fabrication of solid state compact portable pulse power electronics.

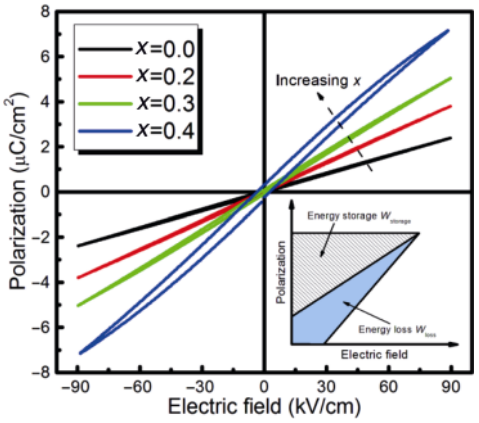

Fig. 4 Polarization–electric field (*P*–*E*) hysteresis loops of $Ba_xSr_{1-x}TiO_3$ (BST, $x \leqslant 0.4$) ceramics. The inset shows the effective energy storage and energy loss during the charge–discharge process. Reproduced with permission from Ref. [37], © Elsevier Ltd and Techna Group S.r.l. 2015.

For aliovalent doping in A-site of ST, a similar phenomenon with giant dielectric TiO_2 can be observed, and corresponding mechanisms are widely studied. Chen *et al.* [41–43] reported (Bi,Sr)TiO_3 ceramics with giant dielectric constant, discussed the related physical mechanisms, and proposed that the first and second ionization of oxygen vacancies as well as corresponding thermal movement were the main reasons. To avoid the problem of Bi-containing oxides volatilizing at high temperature, Shen *et al.* [34,44–46] used trivalent nonvolatile rare earth ions (Re^{3+} = La, Sm, Gd, Er, Nd, etc.) to replace Sr^{2+}, and designed three composition formulas based on three possible charge compensation mechanisms such as equimolar substitution, introducing Sr or Ti vacancy in advance, and successfully fabricated ceramics with perovskite structure. It is experimentally verified the feasibility of introducing ion vacancies in advance for charge compensation, and then the concept of "forced charge compensation mechanism" is summarized and proposed. For instance, Shen *et al.* [44] synthesized $Re_{0.02}Sr_{0.97}TiO_3$ ceramics by introducing Sr vacancy in advance, displaying a high dielectric constant and good bias voltage stability, as shown in Figs. 5 and 6. Furthermore, multiple mechanisms such as Maxwell–Wagner interface polarization, variable charge of Ti element, defect clusters, etc., are all proposed to illustrate donor and/or acceptor doping ST ceramics.

Microstructure regulation plays an important role in enhancing E_b of ST ceramics. In 2014, Song *et al.* [47] prepared $Ba_{0.4}Sr_{0.6}TiO_3$ ceramics with various grain

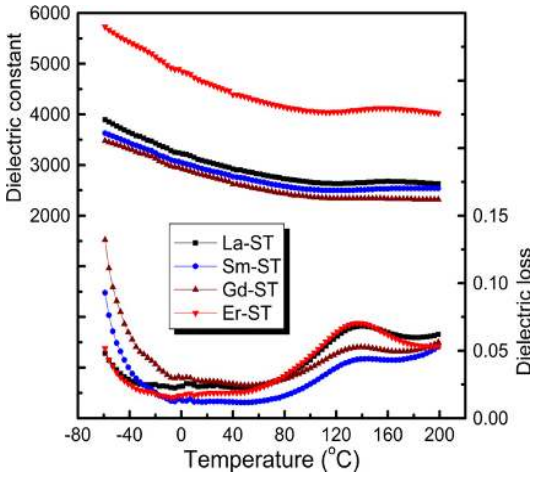

Fig. 5 ε_r and tanδ of the $Re_{0.02}Sr_{0.97}TiO_3$ ceramics as a function of measuring temperature from −60 to 200 ℃. Reproduced with permission from Ref. [44], © The American Ceramic Society 2013.

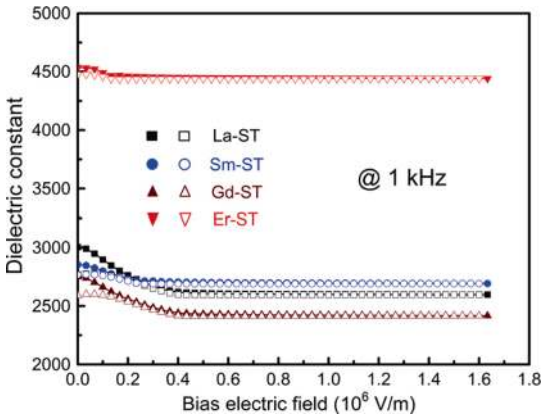

Fig. 6 ε_r of the $Re_{0.02}Sr_{0.97}TiO_3$ ceramics as a function of bias electric field. Filled pattern: increasing bias. Open pattern: decreasing bias. Reproduced with permission from Ref. [44], © The American Ceramic Society 2013.

sizes (0.5–5.6 μm), and observed that dielectric peak gradually depressed and broadened and E_b gradually increased with decreasing grain size, which should be closely related to the ratio of grain/grain boundary and polar nanoregions (PNRs). $Ba_{0.4}Sr_{0.6}TiO_3$ ceramic bulk with grain size of 0.5 μm achieves a high W_{rec} = 1.28 J/cm^3 measured at the highest E_b of 243 kV/cm. Wu *et al.* [48] compared microstructure and energy storage properties of spark plasma sintered (SPS) and conventionally sintered (CS) $Ba_{0.3}Sr_{0.7}TiO_3$ ceramics. The SPS sintered ceramics consists of tetragonal and cubic phases with an average grain size of 880 nm, while CS ones are only of the tetragonal phase. The maximum W_{rec} of SPS samples is 1.13 J/cm^3 at E_b = 230 kV/cm, which is approximately twice as much as that of CS samples (0.57 J/cm^3). In addition, the addition of suitable glass compositions is also an effective method to enhance E_b and reduce the sintering temperature of ST based ceramics [49,50]. In 2019, Shen *et al.* [51] used a homemade glass frit to modify BST enhancing the E_b and reducing the high temperature resistivity, which expanded the working temperature range for energy storage ceramic capacitor applications.

"Defect engineering" is an effective tool to enhance W_{rec} by strengthening relaxor characteristics for ST-based ceramic films. Yang *et al.* [52] fabricated $(Sr_{1-1.5x}Bi_x)Ti_{0.99}Mn_{0.01}O_3$ (SBTM, x = 0.01, 0.05, 0.1) thin films with a thickness of 217 nm using sol–gel method. As x value increases, relaxor behaviors are gradually strengthened due to a slight rotation of the (TiO_6) octahedra induced by the formation of $Bi^{3+}-V''_{Sr}$ defect complex. Under an electric field of 1982 kV/cm,

$(Sr_{0.85}Bi_{0.1})Ti_{0.99}Mn_{0.01}O_3$ possess a W_{rec} of 24.4 J/cm^3 accompanied by the largest ΔP (P_{max}–P_r = 34.3 μC/cm^2). Actually, the introduction of other Bi-contained compounds such as $Bi_{0.5}Na_{0.5}TiO_3$ (BNT) [53], $BiFeO_3$ (BF) [54] has a similar effect to strengthen relaxor characteristics. For example, Pan *et al.* [54] deposited 5 mol% Mn-doped $0.6SrTiO_3$–$0.4BiFeO_3$ (0.6ST–0.4BF) thin film on Nb-doped $SrTiO_3$ single crystal substrate using pulsed laser deposition (PLD), and acquired that W_{rec} and η were 51 J/cm^3 and 64%, respectively. In addition, the energy storage performances exhibited good temperature stability over (−40)–140 ℃ and well fatigue endurance after 2×10^7 cycles. In the related mechanism studies, Hou *et al.* [55] investigated the influence of interface difference and thickness on the energy storage performances for ST thin films, and observed the existence of ionic diffusion layers and oxygen vacancies using high resolution transmission electron microscope (HR-TEM). Moreover, they observed that E_b and P_{max} (up to 10^2 μC/cm^2) along the positive direction were higher than the negative direction. Therefore, a maximum W_{rec} of ST thin films reach 307 J/cm^3 for positive direction, which may be related to local electric field and redistribution of oxygen vacancy.

Various meaningful and interesting works have been done in the optimization of macro/micro structures to improve energy storage properties of ST-based ceramic films. It is well known that the amorphous phase usually possesses higher E_b but lower ε_r than their crystalline counterparts. Gao *et al.* [56] studied energy storage behaviors of amorphous ST thin films with different top electrodes, proposed "self-healing" mechanism based on the anodic oxidation reaction in aluminum electrolytic capacitors. At a relative humidity of 60%, amorphous ST films with Al top electrode achieve the W_{rec} of 15.7 J/cm^3 at 3500 kV/cm, which approaches to 8 times of the samples with Au electrode. Since then, Gao *et al.* [57] inserted insulating Al_2O_3 as a blocking layer to form heterostructure, and achieved a maximum W_{rec} of 39.49 J/cm^3 at E_b = 7542.3 kV/cm when interface number equals 4. Recently, Chen *et al.* [58] used $Ca_{0.2}Zr_{0.8}O_{1.8}$ (CSZ) as dead layer to enhance E_b of $Ba_{0.3}Sr_{0.7}Zr_{0.18}Ti_{0.82}O_3$ (BSZT) thin films. Due to the formation of a high electron injection barrier, Schottky electron emission is suppressed, and thus E_b and W_{rec} are enhanced from 5.4 to 6.3 MV/cm and 64.8 to 89.4 J/cm^3, respectively. Energy storage properties of partially Pb-free linear dielectric ceramics are summarized and listed in Table 1.

In summary, for linear dielectric ceramic bulks, giant dielectric constant can be observed in TiO_2-based with donor/acceptor co-doping at B-site, and ST-based with donor/acceptor co-doping at B-site or aliovalent doping of at A-site bulks by chemical modification. Related physical mechanisms, some controversies, however, are still existed. Energy storage properties of ceramic bulks are limited at expense of a rapid decrease in E_b. Adding of suitable glass phase, special sintering technology and refining grain size are both able to enhance E_b of ceramic bulks. For ST-based ceramic films, adjusting suitable ratio of amorphous and crystalline or introducing a high insulating layer would be a good way to improve its breakdown behavior.

Table 1 Energy storage properties of Pb-free linear dielectric ceramic bulks and films

Composition	Category	t	W_{rec} (J/cm^3)	η (%)	ε_r @ RT	E_b (kV/cm)	Ref.
TiO_2 + 15 wt% BBAS	Bulk	—	1.15	—	103	501.7	[30]
TiO_2	Thick film	0.1 mm	14	—	108	1400	[31]
$Ba_{0.3}Sr_{0.7}TiO_3$	Bulk	0.6 mm	0.23	95.7	650	~90	[37]
$Ba_{0.4}Sr_{0.6}TiO_3$	Bulk	0.3 mm	1.28	—	~1500	243	[47]
$Ba_{0.3}Sr_{0.7}TiO_3$ (SPS)	Bulk	—	1.13	86.8	—	230	[48]
$(Sr_{0.85}Bi_{0.1})Ti_{0.99}Mn_{0.01}O_3$	Thin film	217 nm	24.4	64.7	550	1380	[52]
0.5 mol% Mn-doped 0.6ST–0.4BF	Thin film	500 nm	51	64	240	3600	[54]
ST	Thin film	610 nm	307	89	~350	6600	[55]
Amorphous ST	Thin film	300 nm	15.7	—	29.1	~3500	[56]
ST/4AO	Thin film	370 nm	39.49	—	~15	7542.3	[57]
BSZT	Thin film	610 nm	89.4	65	~160	6300	[58]

BBAS: BaO–B_2O_3–Al_2O_3–SiO_2; ST: $SrTiO_3$; BF: $BiFeO_3$; AO: Al_2O_3; BSZT: $Ba_{0.3}Sr_{0.7}Zr_{0.18}Ti_{0.82}O_3$.

3. 2 Relaxor ferroelectric ceramics

Ferroelectric is a special dielectric material that possesses spontaneous polarization (P_s) at a certain temperature range and the direction of P_s can be changed with an external electric field. Compared with linear dielectric, ferroelectric displays an obvious nonlinear characteristic since the domain cannot fast respond to electric field stimulation. Generally, polarization behavior of dielectric material can be characterized by *P*–*E* loop, and thus ferroelectric can be classified into normal ferroelectric and relaxor ferroelectric [59], as illustrated in Fig. 7. Normal ferroelectric possesses high P_{max} while its high P_r leads to that most of energy is dissipated during the discharge process. By contrast, relaxor ferroelectric exhibits slim *P*–*E* loop with high P_{max} and low P_r (i.e., high $\Delta P = P_{max}–P_r$) meaning that electric energy can be effectively released, and thus obtains better energy storage performances [60]. Note that strengthening the relaxor characteristics and enhancing E_b have become important factors for enhancing W_{rec}. Furthermore, ferroelectric here discussed mainly refers to relaxor ferroelectric.

3.2.1 Pb-based relaxor ferroelectric ceramics

$PbZr_{1-x}Ti_xO_3$ (PZT, $0 \leqslant x \leqslant 1$) ceramic located at morphotropic phase boundary (MPB) where Zr:Ti is of 52:48, possesses a high piezoelectric activity (d_{33} up to 300 pC/N) and good temperature stability, and becomes an extremely popular dielectric material [61–63]. In addition, other ceramic compositions such as PZT 65/35, 70/30 also received more attention and no limitation by piezoelectric properties [64,65]. For example, the researches of actuator in PZT ceramics are increasing due to a large electrostrain under low electric field. In 2019, Kumar *et al.* [66] reported $(Pb_{0.89}La_{0.11})(Zr_{0.70}Ti_{0.30})_{0.9725}O_3$ (PLZT 11/70/30) ceramics achieved a W_{rec} only of 0.85 J/cm^3 due to low electric field. Generally speaking, current energy density of Pb-based relaxor ferroelectric ceramic bulks is less than 3 J/cm^3. In 2017, Zhang *et al.* [67] investigated energy storage properties of $PbZr_{0.52}Ti_{0.48}O_3$-based thin films, acquired a high W_{rec} = 28.2 J/cm^3 for $PbZrO_3$/$PbZr_{0.52}Ti_{0.48}O_3$ bilayer thin films at 2410 kV/cm. In addition, they continued to design a sandwich structure of $PbZr_{0.52}Ti_{0.48}O_3/Al_2O_3/PbZr_{0.52}Ti_{0.48}O_3$ (PZT/AO/PZT) to enhance E_b [68]. Due to the formation of so-called "built-in electric field" at the interface and the high insulating characteristic of AO, PZT/AO/PZT annealed at 550 ℃ achieved a W_{rec} of 63.7 J/cm^3 at 5.7 MV/cm. It should be mentioned that PZT 52/48 system still possesses relatively high P_r restricting its energy storage properties.

Generally, a small amount of La^{3+} (about 7–10 mol%) replacing Pb^{2+} would effectively strengthen the relaxor characteristics of PZT-based ceramics owing to a disrupted long-range ferroelectric order and diffuse phase transition [71,72]. $(Pb,La)(Zr,Ti)O_3$ (PLZT) based relaxor ferroelectric is therefore considered to be a promising energy storage ceramic capacitor candidate. Adjusting suitable La/Zr/Ti ratio generates an important influence on electric properties because of the complicated phase structure. For example, Hu *et al*. [73] investigated the effect of different Zr/Ti ratios on the energy storage properties of PLZT thin films at a fixed La content of 8 mol%. As Ti/(Zr+Ti) ratio gradually increases, ε_r enhances while tanδ shows an opposite trend indicating phase structure gradually transforms from relaxor ferroelectric into normal ferroelectric. At E_b = 2180 kV/cm, W_{rec}, η of the PLZT 8/52/48 relaxor ferroelectric thin films are 30 J/cm^3 and 78%, respectively. In chemical doping, Liu *et al*. [74] used Mn as a dopant of $(Pb_{0.91}La_{0.09})(Zr_{0.65}Ti_{0.35})O_3$ (PLZT 9/65/35) to enlarge the polarization difference of $P_{max}–P_r$, measured a W_{rec} of 30.8 J/cm^3 for 1 mol% Mn

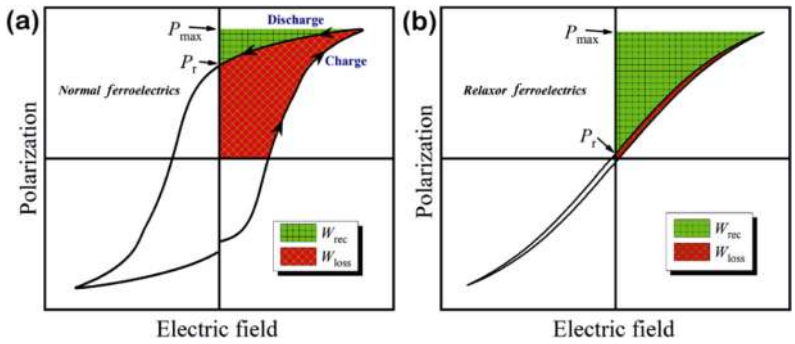

Fig. 7 Schematic of hysteresis loop: (a) normal ferroelectric and (b) relaxor ferroelectric.

thick films. In addition, the addition of excess Pb is a common chemical compensation method to solve the problems of Pb volatilization during the annealing process, and of suppressing the formation of pyrochlore phase [75].

Reasonable design and selection of heterostructure for Pb-based thin films, is an important step in optimizing energy storage properties. In 2013, Zhang *et al*. [76] prepared a compositionally gradient $(Pb_{1-x}La_x)(Zr_{0.65}Ti_{0.35})O_3$ (PLZT, x = 0.08, 0.09, 0.1) thick films using sol–gel method. Up-graded PLZT films possess a W_{rec} of 12.4 J/cm^3 at 800 kV/cm, down-graded one of 8.9 J/cm^3, and the lowest single composition one of 7.1 J/cm^3. It is accepted that high texture quality and dense structure are both severely influencing breakdown behaviors and energy storage performances [77,78]. Nguyen *et al*. [77] deposited $(Pb_{0.9}La_{0.1})(Zr_{0.52}Ti_{0.48})O_3$ (PLZT 10/52/48) thin films using PLD on Si substrate choosing $Ca_2Nb_3O_{10}$ (CNOns) and $Ti_{0.87}O_2$ (TiOns) nanosheets as the template layer. Highly textured (001)-oriented PLZT 10/52/48 films grown on CNOns possess a high W_{rec} of 58.4 J/cm^3, which exceeds W_{rec} of 44 J/cm^3 for (110)-oriented PLZT 10/52/48 films grown on TiOns. Generally speaking, there are differences in lattice constants and thermal expansion coefficients in hetero-interfaces, which provide good conditions for stress. Figure 8(a) shows *P*–*E* loops of PLZT 8/52/48 thick films at different substrates. Ma *et al*. [69] utilized XRD to analyze residual stress for PLZT 8/52/48 thick films, and considered compressive stress can in a certain extent improve tunability of the polarization, enhance E_b and domain switch ability. In addition, note that Peng *et al*. [70] recently prepared Mn-doped $Pb_{0.97}La_{0.02}(Zr_{0.905}Sn_{0.015}Ti_{0.08})O_3$ (PLZST) relaxor ferroelectric thin films, and innovatively proposed a "low-temperature poling" method to improve E_b, and called it "wake-up" mechanism. Figure 8(b) shows *P*–*E* loops of PLZST films before and after "awaken state". E_b and W_{rec} at room temperature are greatly enhanced (nearly doubled) from 1286 to 2000 kV/cm, and from 16.6 to 31.2 J/cm^3, respectively. Energy storage performances of Pb-based relaxor ferroelectric materials are summarized and listed in Table 2.

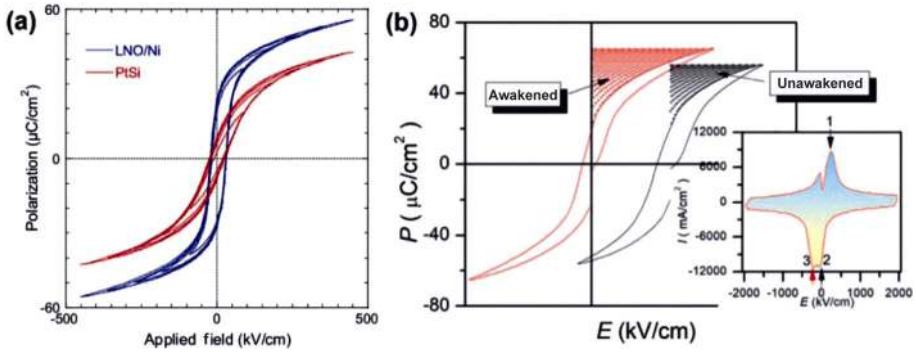

Fig. 8 (a) *P*–*E* loops of the PLZT films on different substrates. Reproduced with permission from Ref. [69], © Springer Science Business Media New York 2015. (b) *P*–*E* loops of the $Pb_{0.97}La_{0.02}(Zr_{0.905}Sn_{0.015}Ti_{0.08})O_3$ films before and after "awaken state", with the inset showing the *I*–*E* curve after "awaken state". Reproduced with permission from Ref. [70], © Elsevier Ltd. 2020.

Table 2 Energy storage properties of Pb-based relaxor ferroelectric ceramic bulks and films

Composition	Category	t	W_{rec} (J/cm^3)	η (%)	ε_r @ RT	E_b (kV/cm)	Ref.
PLZT 11/70/30	Bulk	1 mm	0.85	92.9	~3500	85	[66]
PZ/PZT 52/48	Thin film	350 nm	28.2	~50	—	2615	[67]
PZT/AO/PZT	Thin film	330 nm	63.7	81.3	~50	5711	[68]
PLZT 8/52/48	Thin film	690 nm	30	78	~1500	2180	[73]
1 mol% MnO_2 doped PLZT 9/65/35	Thick film	1.5 μm	30.8	~70	1378	1679	[74]
Up-graded PLZT	Thick film	1.5 μm	12.4	—	2170	800	[76]
PLZT 10/52/48	Thick film	1000 nm	58.4	81.2	—	3400	[77]
PLZT	Thick film	~2 μm	85	65	~1300	~2600	[69]
Low-temperature-poling PLZST	Thin film	320–350 nm	31.2	60	—	2000	[70]

PZ/PZT 52/48: $PbZrO_3/Pb(Zr_{0.52}Ti_{0.48})O_3$; PZT/AO/PZT: $Pb(Zr_{0.52}Ti_{0.48})O_3/Al_2O_3/Pb(Zr_{0.52}Ti_{0.48})O_3$; PLZT 8/52/48: $Pb_{0.92}La_{0.08}(Zr_{0.52}Ti_{0.48})O_3$; PLZT 9/65/35: $(Pb_{0.91}La_{0.09})(Zr_{0.65}Ti_{0.35})O_3$; up-graded PLZT: $(Pb_{1-x}La_x)(Zr_{0.65}Ti_{0.35})O_3$ (x = 0.08, 0.09, and 0.10); PLZT 10/52/48: $Pb_{0.9}La_{0.1}(Zr_{0.52}Ti_{0.48})O_3$; PLZST: $Pb_{0.97}La_{0.02}(Zr_{0.905}Sn_{0.015}Ti_{0.08})O_3$.

3.2.2 Lead-free relaxor ferroelectric ceramics

Lead is a toxic metal, and its volatilization problem at high temperature results in serious environmental and human health concerns. Moreover, some legislation in countries and regions also promote researchers to explore a new lead-free ceramic substitute. Currently, lead-free relaxor ferroelectric ceramics mainly focused on $Bi_{0.5}Na_{0.5}TiO_3$ (BNT), $BaTiO_3$ (BT), $BiFeO_3$ (BF), and $K_{0.5}Na_{0.5}NbO_3$ (KNN) systems, which will be discussed in the following sections.

(1) $Bi_{0.5}Na_{0.5}TiO_3$ based ceramics

$Bi_{0.5}Na_{0.5}TiO_3$ (BNT) is a ferroelectric material firstly discovered by Smolenskii *et al*. [79], which possesses complicated phase structure and good dielectric, piezoelectric, and ferroelectric properties, especially high P_{max} (~40 μC/cm^2) [80–83]. And so it becomes a popular research topic on fundamental theories and practical studies for ferroelectric materials [84–86]. However, the characteristics of high P_r (~38 μC/cm^2), high E_c (~73 kV/cm), and poor sintering behavior for pure BNT ceramics hinder its energy storage applications.

$Bi_{0.5}Na_{0.5}TiO_3$–$x$$BaTiO_3$ (x = 6%–7%) binary solid solution near MPB exhibits excellent electrical properties, and is a most promising candidate for replacing Pb-based ceramics [87–89]. Since then, extensive energy storage studies have been done on this system. It is particularly important that strengthening dynamic of polar nanoregions (PNRs) through disturbing long-range ferroelectric ordering or expanding nonergodic–ergodic phase transition range both could optimize polarization behavior to obtain high W_{rec}. In 2011, Gao *et al*. [90] firstly reported that $0.89Bi_{0.5}Na_{0.5}TiO_3$–$0.06BaTiO_3$–$0.05K_{0.5}Na_{0.5}NbO_3$ (0.89BNT–0.06BT–0.05KNN) ceramics possessed a W_{rec} of 0.46 J/cm^3 at 56 kV/cm. In 2016, Cao *et al*. [91] used Mn^{2+} to modify 0.7(0.94BNT–0.06BT)–0.3ST ceramics to reduce P_r by forming $Mn''_{Ti} - V_{\ddot{O}}$ defect complex, which can induce a local electric field influencing domain switch. A W_{rec} of 1.06 J/cm^3 for 1.1 mol% Mn is obtained at 95 kV/cm owing to a large P_{max}–P_r up to 36.8 μC/cm^2. Actually, similar phenomenon was already reported by Ren *et al*. [92]. In 2017, Li *et al*. [93] incorporated $NaNbO_3$ into $0.8Bi_{0.5}Na_{0.5}TiO_3$–$0.2SrTiO_3$ relaxor ferroelectric ceramics, observed that *P*–*E* loop gradually goes slim together with vanished current peaks as NN content increases, which was attributed to the nonergodic–ergodic phase transition. 0.5 mol $NaNbO_3$ modified ceramics exhibit a high W_{rec} of 0.74 J/cm^3, accompanied by good high temperature energy storage stability and charging–discharging capability. Indeed, delaying the early saturation of polarization is also an effective method to enhance W_{rec} [94]. In our previous work [37,95], $Ba_{0.3}Sr_{0.7}TiO_3$, which is suitable for pulse power systems, is selected to improve energy storage performances of BNT-based with an optimized ceramic composition. *P*–*E* loop of high ε_r $(Ba_{0.3}Sr_{0.7})_{0.35}(Bi_{0.5}Na_{0.5})_{0.65}TiO_3$ ($BS_{0.35}$BNT) relaxor ferroelectric ceramics originally presents an obvious clamped behavior, but its P_r is still high, as shown in Figs. 9(a) and 9(b). We therefore choose

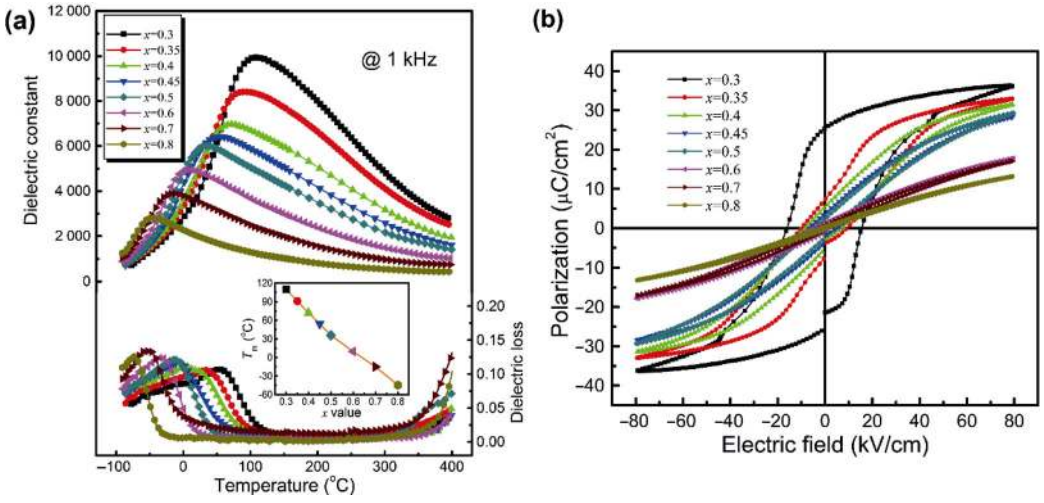

Fig. 9 (a) Temperature dependent dielectric constant and loss of BS_xBNT ceramics. The inset is T_m as a function of x value. (b) *P*–*E* hysteresis loops of the BS_xBNT ceramics with different x value at room temperature. Reproduced with permission from Ref. [95], © The Author(s) 2020.

$NaNbO_3$ (NN) antiferroelectric to continue to optimize its polarization behavior [96]. 0.94BSBNT–0.06NN relaxor ferroelectric ceramics achieve a high W_{rec} of 1.25 J/cm^3 at room temperature. Besides, the system exhibits good high temperature stability and fatigue endurance, which may be closely related to the reduction in domain size.

Besides doping modification, multilayer and miniaturization of BNT-based ceramic capacitors are also a significant research direction. In 2018, Li *et al*. [15] designed a series of $(1-x)Bi_{0.5}Na_{0.5}TiO_3-xSr_{0.7}Bi_{0.2}TiO_3$ (NBT−*x*SBT, x = 0.3–0.5) ceramics, and corresponding multilayer ceramic capacitors (MLCC) with a single layer thickness of 20 μm were fabricated. A high W_{rec} of 9.5 J/cm^3, together with η of 92%, is achieved in NBT–0.45SBT MLCC. Furthermore, energy storage properties of MLCC display good temperature stability, fatigue endurance, and charging–discharging capability. Recently, Li *et al*. [97] attempted to enhance E_b through controlling grain orientation, and investigated energy storage performances of NBT–0.35SBT MLCC under different stress states. By comparison, Yang *et al*. [98] reported energy storage properties of gradient structure ($SrTiO_3$ + 0.5 wt% Li_2CO_3)/($0.93Bi_{0.5}Na_{0.5}TiO_3$–$0.07Ba_{0.94}La_{0.04}Zr_{0.02}Ti_{0.98}O_3$) (STL/(BNT–BLZT)) ceramics along thickness direction. A high W_{rec} of 2.72 J/cm^3 for STL/(BNT–BLZT) ceramics is obtained at 294 kV/cm. Due to the strict requirements of the harsh working environment such as high temperature (> 200 ℃ or even 300 ℃), good insulation and antioxidant, MLCC would encounter many challenges in the future [99,100]. Meanwhile, material system selection, electrode design such as equivalent series resistance (ESR) and loss, cost control of fabrication, and so on, need further consideration.

The volatilization of Bi and Na and variable valence of Ti are easy to generate oxygen vacancy for BNT-based thin films resulting in a large leakage current. Single mental oxides (MnO_2 [101,102], Fe_2O_3 [103], etc.) are used to modify BNT films, which would form different defect complexes to compensate charge balance and suppress oxygen vacancy migration. For example, Mn doped BNT thick films display a reduced leakage current due to the formation of $Mn''_{Ti}-V_{\ddot{O}}$. defect complex, which gives rise to a W_{rec} of 30.2 J/cm^3 for x = 0.01 composition [102]. In addition, controlling annealing temperature also has a similar effect on reducing leakage current [104]. In addition, Peng *et al*. [105] deposited La/Zr modified 0.94BNT–0.06BT high epitaxial quality thin films using PLD, and P_{max} can reach to 10^2 μC/cm^2 scale due to the complicated phase composition and great relaxor dispersion. (100) and (111) oriented $(Bi_{1/2}Na_{1/2})_{0.9118}La_{0.02}Ba_{0.0582}(Ti_{0.97}Zr_{0.03})O_3$ (BNLBTZ) thin films achieve maximum W_{rec} of 137 and 154 J/cm^3, respectively, far exceeding other Pb-free even Pb-based systems.

Distinguished from single composition of MLCC, macrostructure modification of BNT-based films mainly focuses on gradient composition. It is widely accepted that BNT-based ceramic film is p-type conductivity due to many vacancies generating acceptor states in the band gap, and thus p–n junctions and block layers are applied to inhibit charge transportation. For instance, Guo *et al*. [108] reported the introduction of $Bi_{3.25}La_{0.75}Ti_3O_{12}$ (BLT) and $Pb(Zr_{0.4}Ti_{0.6})O_3$ (PZT) dielectric layer on pyroelectric and ferroelectric properties of 0.94BNT–0.06BT ceramic films, and observed leakage current reduce about 3 orders of magnitude. Besides, Chen *et al*. [106] studied the effect of interface number on energy storage properties of $0.94(Bi_{0.5}Na_{0.5})TiO_3$–$0.06BaTiO_3/BiFeO_3$ (abbreviated as BNBT/*n*BFO) multilayer film capacitors under a given total thickness. BNBT/2BF thin films exhibit a W_{rec} of 31.96 J/cm^3 and a η of 61% at 2400 kV/cm owing to enhanced insulating characteristic and high polarization. With the rapid development of flexible wearable materials in recent years, related researches on their energy storage performances have gradually increased. Qian *et al*. [107] prepared a multilayer $(Na_{0.8}K_{0.2})_{0.5}Bi_{0.5}TiO_3/0.6(Na_{0.8}K_{0.2})_{0.5}Bi_{0.5}TiO_3$–$0.4SrTiO_3$ $(NKBT/NKBT–ST)_N$ (N = 2, 3, 6, 8) films on the F-Mica substrate, with measured W_{rec} of 73.7 J/cm^3 at 3077 kV/cm for N = 6. Under different conditions such as (−50)–200 ℃, 10^8 cycle numbers, 10^4 bending tests, energy storage performances of $(NKBT/NKBT–ST)_6$ ceramic films both maintain good stability. Energy storage performances of BNT-based relaxor ferroelectric materials are summarized and listed in Table 3.

(2) $BaTiO_3$-based ceramics

$BaTiO_3$ (BT) with simple perovskite structure possesses moderate Curie temperature (T_C) of 120 ℃ and corresponding high ε_r of 10^4 [109,110], and becomes a common dielectric material in passive capacitor. BT-based materials also received more attention in memory and memristor for information

Table 3 Energy storage characteristics of BNT-based relaxor ferroelectric ceramic bulks and films

Composition	Category	t	W_{rec} (J/cm^3)	η (%)	ε_r @ RT	E_b (kV/cm)	Ref.
0.89BNT–0.06BT–0.05KNN	Bulk	0.5 mm	0.46	—	~2000	56	[90]
1.1 mol% Mn doped 0.7(0.94NBT–0.06BT)–0.3ST	Bulk	—	1.06	—	—	95	[91]
0.95(0.8BNT–0.2ST) –0.05NN	Bulk	—	0.74	55	~2000	70	[93]
$0.94BS_{0.35}$BNT–0.06NN	Bulk	0.3–0.35 mm	1.25	76	~3800	116	[96]
0.55BNT–0.45SBT	Bulk	20 μm @ SL	9.5	92	~2500	720	[15]
STL/(BNT–BLZT)	Bulk	0.2 mm	2.72	74	~900	294	[98]
0.01 mol Mn doped BNT	Thick film	1200 nm	30.2	47.7	~400	2310	[102]
(111)-oriented BNLBTZ	Thin film	350 nm	154	95	~2000	3500	[105]
0.94BNT–0.06BT/2BF	Thin film	400 nm	31.96	61	~500	2400	[106]
$(NKBT/NKBT–ST)_{N=6}$	Thin film	260 nm	73.7	68.1	~600	3072	[107]

BNT: $Bi_{0.5}Na_{0.5}TiO_3$; BT: $BaTiO_3$; KNN: $K_{0.5}Na_{0.5}NbO_3$; ST: $SrTiO_3$; NN: $NaNbO_3$; $BS_{0.35}$BNT: $(Ba_{0.3}Sr_{0.7})_{0.35}(Bi_{0.5}Na_{0.5})_{0.65}TiO_3$; SBT: $Sr_{0.7}Bi_{0.2}TiO_3$; STL/(BNT–BLZT): $(SrTiO_3 + 0.5wt\%Li_2CO_3)/(0.93Bi_{0.5}Na_{0.5}TiO_3–0.07Ba_{0.94}La_{0.04}Zr_{0.02}Ti_{0.98}O_3)$; BNLBTZ: $(Bi_{1/2}Na_{1/2})_{0.9118}La_{0.02}Ba_{0.0582}(Ti_{0.97}Zr_{0.03})O_3$; BF: $BiFeO_3$; NKBT: $(Na_{0.8}K_{0.2})_{0.5}Bi_{0.5}TiO_3$. SL means single layer.

storage and transfer. In addition, the structure and physical property research of BT-based materials still attract more attentions [111–113]. However, pure BT ceramic has some problems such as high P_r, the reduction from Ti^{4+} to Ti^{3+} at high temperature, which restrict it to achieve high W_{rec} [114].

In 2009, Ogihara *et al*. [115] synthesized a temperature stable $0.7BaTiO_3–0.3BiScO_3$ (0.7BT–0.3BS) relaxor ferroelectric ceramics with a thickness of 0.2 mm, and obtained W_{rec} of 2.3 J/cm^3 at 225 kV/cm. When thickness reduces to 15 μm, W_{rec} enhances to 6.1 J/cm^3 at 730 kV/cm. By comparison, Wu *et al*. [116] utilized $BiScO_3$ (BS) as shell material to coat BT, and W_{rec} only of 0.68 J/cm^3 was measured at E_b = 120 kV/cm for BT@3 mol% BS ceramics. Yuan *et al*. [117] prepared $Bi(Mg_{1/2}Zr_{1/2})O_3$ (BMZ) modified BT-based relaxor ferroelectric, and achieved a high W_{rec} = 2.9 J/cm^3 for 0.85BT–0.15BMZ ceramics higher than pure BT ceramics (0.4 J/cm^3), and corresponding *P*–*E* loop is exhibited in Fig. 10(a). The authors thought the enhancement of W_{rec} is related to PNRs, as evidenced by piezoelectric force microscope (PFM) and transmission electron microscope (TEM). It should be mentioned that other systems such as $BaTiO_3–Bi(Mg,Ti)O_3$ (BT–BMT) also display good energy storage capabilities due to the low tolerance factor of Bi-based compound [118,119]. In recent years, $Ba_{0.85}Ca_{0.15}Zr_{0.10}Ti_{0.90}O_3$ (BCZT) based relaxor ferroelectric gains more attention in ferroelectric and pyroelectric properties because of high ε_r at room temperature [120–123]. However, W_{rec} of BCZT-based ceramic bulks is commonly less than 3 J/cm^3 limited to a low E_b. If the trade-off relationship between ε_r and E_b gets a good balance, BCZT-based ceramics would be a promising energy storage candidate.

"Core–shell" structure is a common way of modifying BT-based ceramics, especially in enhancing temperature stability for ceramic capacitor applications. In 2014, Su *et al*. [124] coated BT nanocrystals with $65PbO–20B_2O_3–15SiO_2$ and $65Bi_2O_3–20B_2O_3–15SiO_2$ glass phases, reducing sintering temperature to 900 ℃. Meanwhile, the authors estimated W_{rec} approaching to 10 J/cm^3 by equation for Bi-based glass phase. Similarly, high E_b materials such as SiO_2 [125] and $SrTiO_3$ (ST) [126] are both used as shell materials to improve breakdown behavior. For example, Wu *et al*. [126] fabricated BT@ST relaxor ferroelectric ceramics using the sol-precipitation approach, and EDS analysis illustrated BT@ST ceramics in Fig. 10(b). However, with a W_{rec} only of 0.22 J/cm^3 at 47 kV/cm, η approaches to 90%. It should be pointed that high E_b materials usually possess low ε_r, and so W_{rec} of coated BT ceramics cannot be effectively enhanced at the sacrifice of ε_r. Bi-based materials such as $BiScO_3$ as shell material also suffer from the same problem of obtaining high W_{rec}. The reason needs to be further explored due to the complex composition gradient.

$Ba(Zr,Ti)O_3$ (BZT) based ceramic films are considered to be a potential energy storage material since Zr^{4+} has a stable valence and similar ion radius of Ti^{4+}, as well as good relaxor characteristics. As Zr^{4+} content increases, relaxor degree gradually enhances, and a weak diffuse phase transition accompanying slim *P*–*E* loop can be founded when Zr^{4+} near 15 mol%, which is attributed to the inhomogeneous distribution of Zr and mechanical stress [128,129]. Therefore, energy

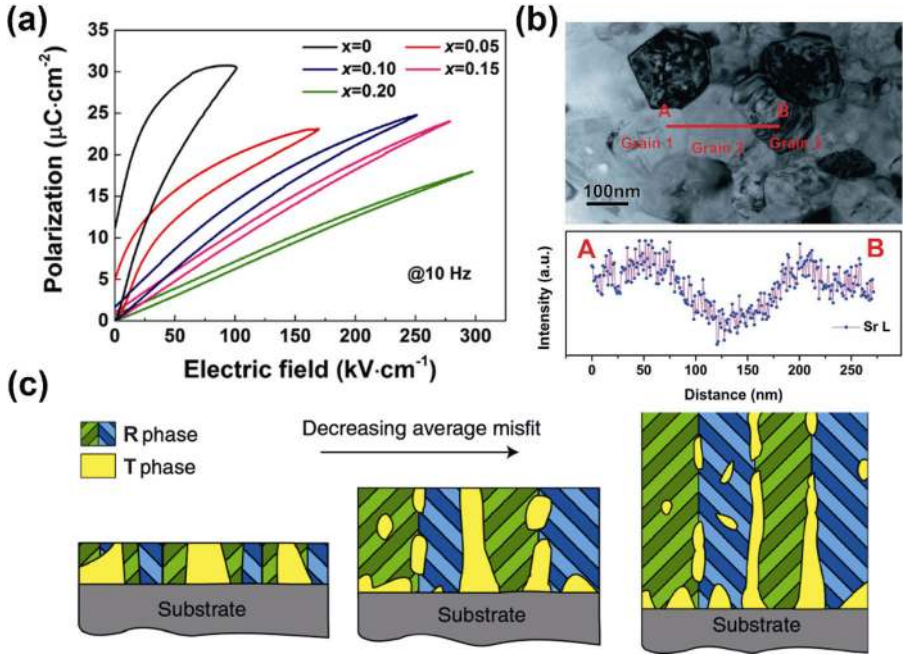

Fig. 10 (a) *P–E* loop of $BaTiO_3$–$xBi(Mg_{1/2}Zr_{1/2})O_3$ at room temperature. Reproduced with permission from Ref. [117], © Elsevier Ltd. 2018. (b) EDS line scanning analysis of Sr in the BT@ST ceramic. Reproduced with permission from Ref. [126], © The Royal Society of Chemistry 2015. (c) Schematic of the microstructure evolution with film thickness for $Ba(Zr_{0.2},Ti_{0.8})O_3$ thin films. Reproduced with permission from Ref. [127], © The Author(s) 2017.

storage performances of BZT-based ceramic systems receive more attention. Instan *et al*. [130] prepared 400 nm <100>-oriented $Ba(Zr_xTi_{1-x})O_3$ (x = 0.3, 0.4, 0.5) relaxor ferroelectric thin films using PLD on $La_{0.7}Sr_{0.3}MnO_3$/MgO substrates. Importantly, W_{rec} of all ceramics can reach a scale of 10^2 around $E_b \approx$ 3 MV/cm, and a maximum W_{rec} of 156 J/cm^3 is obtained at x = 0.3 composition. In 2017, Cheng *et al*. [127] reported the influence of thickness and substrate categories on domain/phase of $Ba(Zr_{0.2}Ti_{0.8})O_3$ thin films. With increasing thickness, mismatch stress gradually releases and rhombohedral phase content increases, as well as twined domain structure is formed, as shown in Fig. 10(c). A high W_{rec} of 166 J/cm^3 for $Ba(Zr_{0.2}Ti_{0.8})O_3$ thin films is achieved at $E_b \approx$ 5.7 MV/cm. In addition, oxygen pressure is found to generate a positive effect on energy storage properties of BT-based thin films [131].

"Interface engineering", including interface compatibility, periodic number, and space charge, plays a critical role in enhancing E_b and optimizing polarization behavior of BT-based ceramic films. In 2012, Ortega *et al*. [132] deposited $BaTiO_3/Ba_{0.3}Sr_{0.7}TiO_3$ superlattice thin films on MgO single substrate using PLD, and acquired a W_{rec} of 12.24 J/cm^3 measured by *P–E* loop. It should be noted that a theoretical value of W_{rec} = 46 J/cm^3 at E_b reach to 5.8–6 MV/cm. Sun *et al*. [133] studied energy storage properties of laminated $Ba_{0.7}Ca_{0.3}TiO_3/BaZr_{0.2}Ti_{0.8}O_3$ (BCT/BZT) thin films with two layers as a period and the number is 2, 4, 8. With increasing period, E_b enhances from 3 to 4.5 MV/cm, and a maximum W_{rec} is 52.4 J/cm^3 for N = 8. Meanwhile, a series of multilayer structures consisting of two materials or a stack of different dielectric layers, have become the most charming model systems since some unique properties can be enhanced. Due to the difference of electric properties in stacked dielectric material, some physical mechanisms such as current leakage mechanism and charge distribution in heterostructure interface, still need to be further investigated [134,135]. Energy storage performances of the BT based relaxor ferroelectric materials are summarized and listed in Table 4.

(3) $BiFeO_3$-based ceramics

$BiFeO_3$ (BF) as a multiferroic material with perovskite structure exhibits high T_C (~850 ℃), high P_s (~100 μC/cm^2), and large S_{max} (~0.4 %), and gains extensive studies in different cross fields such as piezoelectric, magnetic, and quantum [136–139]. The volatile nature of Bi and multiple valence variation of Fe during sintering cause large dielectric loss and leakage current [140]. Nevertheless, BF relaxor ferroelectric is

Table 4 Energy storage properties of BT-based relaxor ferroelectric ceramic bulks and films

Composition	Category	t	W_{rec} (J/cm^3)	η (%)	ε_r @ RT	E_b (kV/cm)	Ref.
0.7BT–0.3BS	Bulk	0.2 mm	2.3	—	~900	225	[115]
	Thick film	15 μm	6.1	—	750–800	730	
BT@3BS	Bulk	—	0.68	81	~1500	120	[116]
0.85BT–0.15BMZ	Bulk	0.2 mm	2.9	86.8	~1000	279.8	[117]
BT with BBS glass	Bulk	—	~10	—	~550	~1140	[124]
BT@ST	Bulk	—	0.22	~90	~2000	47	[126]
<100>-oriented $Ba(Zr_{0.3}Ti_{0.7})O_3$	Thin film	400 nm	156±1	72.8	~3400	3000	[130]
$Ba(Zr_{0.2}Ti_{0.8})O_3$	Thin film	350 nm	166	~90	~350	5700	[127]
Superlattice BT/BST	Thin film	0.6 μm	~12.24	—	~800	1660	[132]
$(BCT/BZT)_{N=8}$	Thin film	100 nm	52.4	72.3	~175	4700	[133]

BT: $BaTiO_3$; BS: $BiScO_3$; BMZ: $Bi(Mg_{1/2}Zr_{1/2})O_3$; BBS: $65Bi_2O_3$–$20B_2O_3$–$15SiO_2$; ST: $SrTiO_3$; BST: $Ba_{0.3}Sr_{0.7}TiO_3$; BCT: $Ba_{0.7}Ca_{0.3}TiO_3$; BZT: $BaZr_{0.2}Ti_{0.8}O_3$.

still considered as a potential candidate for energy storage capacitors because of high P_s.

$BiFeO_3$–$x$$BaTiO_3$ (BF–xBT, $0 \leqslant x \leqslant 0.5$) ceramics maintain high T_C, good ferroelectric and piezoelectric properties resulted from complicated phase structure evolution. With increasing x value, BF–xBT ceramics possess a high P_{max} near MPB of BT $\approx$ 0.33 mol [141–143]. Energy storage properties of BF-based ceramics, therefore, basically are around BF–0.33BT system to reduce P_r. For example, Liu *et al*. [144] added $Ba(Zn_{1/3}Ta_{2/3})O_3$ (BZT) into BT–0.34BT relaxor ferroelectric ceramics obtaining a W_{rec} of 2.56 J/cm^3 at 160 kV/cm. To enhance breakdown strength of BF-based ceramics, Qi *et al*. [145] introduced $NaNbO_3$ (NN) combined with 0.1 wt% MnO_2 and 2 wt% $BaCu(B_2O_5)$ (BCB) as sintering aids to modify 0.67BF–0.33BT relaxor ferroelectric ceramics, and corresponding Weibull distribution of E_b is given in Fig. 11(a). At 360 kV/cm, x = 0.1 sample possesses a maximum W_{rec} of 8.12 J/cm^3 accompanied to η of 90%, which is related to the existence of nanodomain and high density. In addition, Wang *et al*. [146] reported that W_{rec} of 0.62BF–0.3BT–0.08$Nd(Zr_{0.5}Zn_{0.5})O_3$ ceramic bulks is 2.45 J/cm^3 at 240 kV/cm. When an MLCC device based on this system is made, W_{rec} is enhanced to 10.5 J/cm^3.

Similar to BF–xBT systems, ST modified BF-based energy storage ceramics are mainly concentrated on films due to thickness limitation. In 2013, Correia *et al*. [147] prepared 0.4BF–0.6ST thin films using PLD, obtained a high W_{rec} of 18.6 J/cm^3 at 972 kV/cm. Recently, Pan *et al*. [148] reported (0.55–x)BF–xBT–0.45ST (x = 0–0.4) thin films with polymorphic nanodomain structure are grown on Nb-doped $SrTiO_3$ single crystal substrate. Under an electric field of 4.9 MV/cm, x = 0.3 composition achieves a maximum

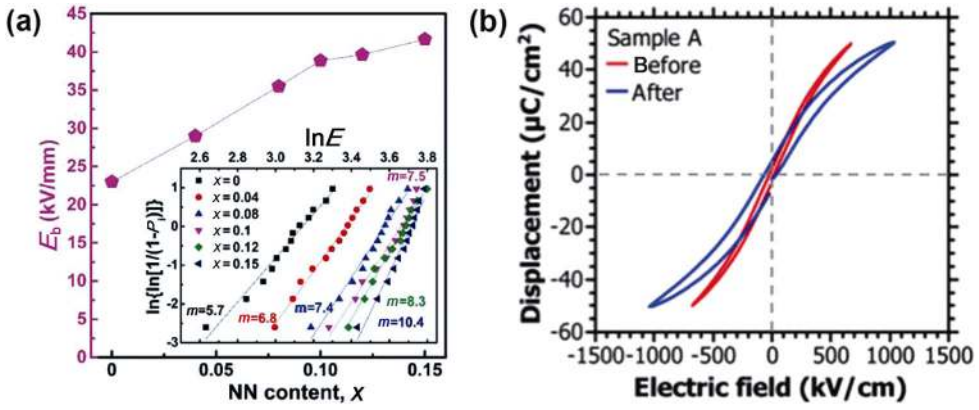

Fig. 11 (a) Weibull distribution and calculated E_b values of (0.67−x)BF–0.33BT–xNN ceramics. Reproduced with permission from Ref. [145], © WILEY-VCH Verlag GmbH & Co. KGaA, Weinheim 2019. (b) P–E loops from two film capacitor structures before and after the introduction of an alumina layer at the electrode–0.6BF–0.4ST interface. Reproduced with permission from Ref. [150], © AIP Publishing 2012.

W_{rec} =112 J/cm^3 more than 53 J/cm^3 of pure 0.55BF–0.45ST thin films, which is owing to the enhanced relaxor behaviors and breakdown strengthen. Moreover, the energy storage performances of this system maintain good stability in a wide temperature range of (−100)–150 ℃ and 10^8 cycles, respectively. In addition, an important and interesting double *P*–*E* loop can be observed in rare earth substituted BF thin films due to the transition from orthorhombic to rhombohedral phase [149].

In heterostructure design, McMillen *et al*. [150] firstly proposed to use "artificial dead layer" to enhance E_b, deposited Al_2O_3 layer with 6 nm between 0.6BF–0.4ST film and ST substrate, and corresponding *P*–*E* loops before and after inserting Al_2O_3 layer were illustrated in Fig. 11(b). Interface polarization behavior to some degree increases hysteresis loss while Al_2O_3 insulating layer enhances E_b, and thus W_{rec} enhances from 13 to 17 J/cm^3. Since then, a sandwich structure of "soft layer" with high polarization and "hard layer" with high E_b are constructed to prevent "electric tree" growth and achieve high W_{rec} [151]. It is particularly important that strong interface coupling factors should be considered in designing structure and analyzing properties [152]. Energy storage performances of the BF-based relaxor ferroelectric materials are summarized and listed in Table 5.

(4) $K_{0.5}Na_{0.5}NbO_3$-based ceramics

$K_{0.5}Na_{0.5}NbO_3$ (KNN) is a binary solid solution of $KNbO_3$ ferroelectric and $NaNbO_3$ antiferroelectric, and possesses a moderate d_{33} around 80 pC/N, high T_C of 420 ℃, and complicated phase structure [153,154]. Since the 1950s at latest century, the researches of KNN materials concentrate on piezoelectric properties due to MPB located at $KNbO_3$ content of 47.5% [154]. The ratio of K/Na has a slight variation while mainly concentrated on 0.5/0.5. However, narrow sintering temperature range, easy volatilization characteristic of K, Na at high temperature both hinder its applications.

In 2016, Du *et al*. studied KNN-based energy storage ceramics, and achieved a high W_{rec} of about 4 J/cm^3 for $SrTiO_3$ (ST) [155] and $Bi(Mg_{1/3}Nb_{2/3})O_3$ (BMN) [156] modified KNN ceramics. And they further used CuO [157], ZnO [158], etc., as fruit to improve sintering behavior of KNN-based ceramics. It should be noted that modified KNN-based energy storage ceramics with superfine grain size possess not only high E_b but also good transparency. In addition, utilize "phase boundary engineering" of KNN ceramics to enhance electric properties is a useful method. Recently, Yang *et al*. [159] proposed "morphotropic relaxor boundary (MRB)" in BT modified KNN ceramics to illustrate an obvious enhancement of electrostrain and dielectric permittivity. At the MRB the electrostrain increases by ~3 times and the permittivity increases by ~1.5 times over a wide temperature range of more than 100 K, as compared with off-MRB compositions. In comparison, the studies of KNN-based ceramic films for energy storage are relatively less, which should be related to insolubility of Nb and volatilization of K and Na. In 2017, Won *et al*. [160] reported 6 mol% $BiFeO_3$-doped $(K_{0.5},Na_{0.5})(Mn_{0.005},Nb_{0.995})O_3$ (KNMN) thick film possessed a slim *P*–*E* loop, and achieved a W_{rec} of 28 J/cm^3, η of 90.3%. Recently, Huang *et al*. [161] also used MnO_2 to reduce leakage current of $0.95(K_{0.49}Na_{0.49}Li_{0.02})(Nb_{0.8}Ta_{0.2})O_3$–$0.05CaZrO_3$−$x$ mol% Mn (KNN–LT–CZ5−x mol% Mn) thin films prepared by sol–gel methods, and achieved a high W_{rec} = 64.6 J/cm^3 under an electric field of 3080 kV/cm at x = 0.5 composition. Energy storage properties of KNN-based relaxor ferroelectric ceramics and films are summarized and listed in Table 6.

In summary, for relaxor ferroelectric ceramics, the formation of PNRs due to disturbed long-range ferroelectric order or nonergodic–ergodic phase transition can strengthen relaxor characteristics. Reflecting on macroscopic ferroelectric properties, *P*–*E* loop goes

Table 5 Energy storage properties of BF-based relaxor ferroelectric ceramic bulks and films

Composition	Category	t	W_{rec} (J/cm^3)	η (%)	ε_r @ RT	E_b (kV/cm)	Ref.
0.6BF–0.34BT–0.06BZT	Bulk	0.2 mm	2.56	~70	—	160	[144]
0.57BF–0.33BT–0.1NN	Bulk	0.15 mm	8.12	90	—	360	[145]
0.62BF–0.3BT–0.08NZZ	Bulk	16 μm @ SL	10.5	87	—	700	[146]
0.4BF–0.6ST	Thin film	400 nm	18.6	>85	~900	972	[147]
0.25BF–0.3BT–0.45ST	Thin film	450–500 nm	112	80	~250	4900	[148]
Dead layer engineered 0.6BF–0.4ST	Thin film	400 nm	17	—	—	—	[150]

BF: $BiFeO_3$; BT: $BaTiO_3$; BZT: $Ba(Zn_{1/3}Ta_{2/3})O_3$; NN: $NaNbO_3$; NZZ: $Nd(Zn_{0.5}Zr_{0.5})O_3$; ST: $SrTiO_3$. SL means single layer.

Table 6 Energy storage properties of KNN-based relaxor ferroelectric ceramic bulks and films

Composition	Category	t	W_{rec} (J/cm^3)	η (%)	ε_r @ RT	E_b (kV/cm)	Ref.
0.85KNN–0.15ST	Bulk	0.2 mm	4.03	~52	~1500	400	[155]
0.90KNN–0.10BMN	Bulk	0.2 mm	4.08	62.7	~1000	300	[156]
$BiFeO_3$-doped KNMN	Thick film	1 μm	28	90.3	—	2000	[160]
5 mol% Mn-doped KNN–LT–CZ5	Thin film	650 nm	64.6	84.6	—	3080	[161]

ST: $SrTiO_3$; BMN: $Bi(Mg_{2/3}Nb_{1/3})O_3$; KNMN: $(K_{0.5},Na_{0.5})(Mn_{0.005},Nb_{0.995})O_3$; KNN–LT–CZ5: $0.95(K_{0.49}Na_{0.49}Li_{0.02})(Nb_{0.8}Ta_{0.2})O_3$–$0.05CaZrO_3$

slim. In addition, delay saturated polarization is also used to optimize polarization behavior. Designing multilayer ceramic capacitor (MLCC), "core–shell" structure with non-ferroelectric phase as shell material is commonly accepted method to improve electric breakdown behavior for ceramic bulks. By comparison, chemical modification of ceramic films functions two roles: For one, suppress the generation and transportation of vacancy defect to reduce leakage current; for the other one, strengthen its relaxor characteristics and optimize polarization behavior. In the heterostructure of ceramic films, match degree of physical paraments such as lattice constant, thermal expansion coefficient, etc., gradient sequence, template or new inert layers are all important factors to influence energy storage performances.

3. 3 Antiferroelectric ceramics

As a special group of ferroelectric material, antiferroelectric has many similarities with ferroelectric whereas still exists obvious differences. In 1951, Kittel [162] originally proposed the concept of antiferroelectric, predicted the existence, and gave some basic characteristics. Generally speaking, antiferroelectric materials possess P_s in a unit cell, but the direction of P_s is antiparallel to that of neighboring unit cell. Antiferroelectric, therefore, does not exhibit polarization in macroscopic characteristics. It is particularly important that antiferroelectric exists a unique feature: double hysteresis loop under an external field. P is linearly proportional to E at a low electric field. When E exceeds the forward switching (AFE-to-FE) field $E_{A–F}$, antiferroelectric displays an obvious ferroelectric behavior, and P fastly increases and gradually reaches P_{max}. Note that antiferroelectric can undergo a ferroelectric–antiferroelectric phase transition field ($E_{F–A}$) after removing E. Consequently, P gradually reduces and returns to the initial state (that is, $E = 0$, $P_r = 0$). A similar variation in P can be observed as E continuously increases in an opposite direction.

It is hard to see a double hysteresis loop for most pure antiferroelectric materials at a low electric field, which usually requires special conditions of high temperature and strong electric field to stimulate. Thereby, it is a crucial challenge for antiferroelectric to obtain double P–E loop especially for ceramic bulks. In addition, a typical high squareness P–E loop, and corresponding internal strain induced by antiferroelectric–ferroelectric phase transition both result in low W_{rec} and reduced device life [12]. In this regard, how to stabilize and relax the antiferroelectric phase (corresponding to enhancing $E_{A–F}$, reducing the difference of $E_{A–F}$–$E_{F–A}$) and enhance E_b has become a particularly important issue to acquire good energy storage performances.

3.3.1 Pb-based antiferroelectric ceramics

(1) $PbZrO_3$

$PbZrO_3$ (PZ) is the prototype antiferroelectric, and serves as a model system to be thoroughly studied so far. The origin of the phase transition mechanism, however, is not well understood [163]. Despite this, a characteristic double P–E loop with high P_{max} and low P_r makes it suitable for energy storage capacitors. PZ-based energy storage ceramics gain increasing attention since Chen *et al*. [164] reported W_{rec} of 7.1 J/cm^3 for PZ thin films during phase transition, but basically around ceramic films.

It is widely accepted that tolerance factor t of perovskite structure is closely related to phase stability, and the equation is represented as

$$t = \frac{r_A + r_O}{\sqrt{2}\left(r_B + r_O\right)} \tag{10}$$

where r_A, r_B, r_O denote ion radius of A, B, and O, respectively. In general, AFE phase can be stabilized for $t < 1$, and reducing t can enhance in some degree the stability of AFE phase. For example, Hao *et al*. [165] substituted Pb^{2+} (1.20 Å) with smaller Sr^{2+} (1.12 Å) to reduce t, and P–E loop goes slim together with increased $E_{A–F}$ and decreased ΔE. As a consequence, $(Pb_{0.95}Sr_{0.05})ZrO_3$ (PSZ5) thin films obtain a W_{rec} of

14.5 J/cm^3. Choosing smaller ion radius while aliovalent of La^{3+} as donor dopant has a similar effect [166]. In addition, controlling the orientation of PZ thin film also achieves the purpose of stabilizing the antiferroelectric phase. PZ thin film with (100) orientation needs a higher electric field than with (111) one to finish antiferroelectric–ferroelectric phase transition [167].

Tailoring local electric field and stress to enhance W_{rec} is hard but interesting work. As is well known, introducing a new nanoparticle in materials often brings novel properties and improved properties. For example, Sa *et al*. [169] used α-Fe_2O_3 nanoparticles to modify PZ thin films, obtained a W_{rec} of 17.4 J/cm^3 and P_{max} as high as 78 μC/cm^2 attributing to the local field effect. By comparison, Chen *et al.* [170] fabricated a self-assembled PZ:NiO nano-columnar composite using PLD, and proposed that tensile stress mainly comes from the interface of two phases. At E_b = 1000 kV/cm, 5 vol% NiO thin films possess a high P_{max} of ~91 μC/cm^2, and W_{rec} of 24.6 J/cm^3. Meanwhile, Ge *et al*. [171,172] also did a series of works on optimizing polarization behavior mainly such as enhancing P_{max}, reducing $E_{A–F}$–$E_{F–A}$ using the stress engineering method. To our best knowledge, it is difficult to directly measure and characterize local electric field and stress, and thus corresponding methods need to be developed. Furthermore, the gradient sequence of thin film is significant for enhancing W_{rec}. Ye *et al*. [168] reported a W_{rec} of 16.3 J/cm^3 for down-graded higher than that of 9.7 J/cm^3 for up-graded PZ-based thin films, and corresponding *P*–*E* loops are shown in Fig. 12.

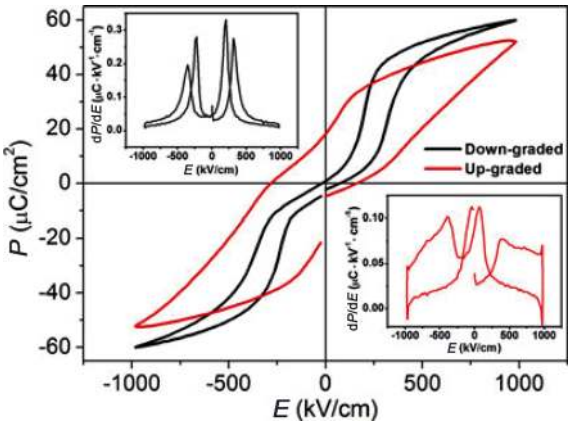

Fig. 12 *P*–*E* loops of up- and down-graded Eu-doped PZ thin films. Inset: the differentiated *P*–*E* hysteresis loops of down- and up-graded thin films, respectively. Reproduced with permission from Ref. [168], © The American Ceramic Society 2012.

It should be mentioned that $PbHfO_3$ (PHO) antiferroelectric ceramics have some similarity with PZO, and thus the related studies still concentrate on phase structure [173–175]. Nevertheless, the energy storage properties of PHO-based ceramics have rarely been reported. In 2020, Chao *et al*. [176] prepared $Pb_{0.98}La_{0.02}(Hf_xSn_{1–x})_{0.995}O_3$ antiferroelectric ceramics, and achieved a good energy storage performance: W_{rec} and η are of 7.63 J/cm^3 and 94% for x = 0.45 composition, respectively. Recently, Huang *et al*. [177] reported pure PHO ceramic films by sol–gel method at 650 ℃ annealing temperature, and achieved a W_{rec} of 24.9 J/cm^3.

(2) (Pb, La)(Zr, Sn, Ti)O_3

As discussed in Section 3.2.1, $Pb(Zr_{1–x}Ti_x)O_3$ (PZT, $x \approx 0.05$) solid solutions located at rich Zr regions of ferroelectric–antiferroelectric (FE–AFE) phase boundary, exhibit rich phase structures and well electrical properties [61,62]. It is worth noting that PZT systems at FE–AFE phase boundary differ from MPB in electric properties. For instance, FE and AFE cannot be transformed into each other under force or electric field, while temperature, stress, or other factors induced by FE–AFE phase transition can occur. Meanwhile, the region of the antiferroelectric phase for PZT 95/5 is relatively narrow, and a slight composition fluctuation would easily cause deviation from FE–AFE phase boundary.

La^{3+} and Sn^{4+} are very popular A/B site dopants in PZT 95/5 ceramics where their functions are similar [178–182]. La^{3+}, as a donor dopant, substitutes Pb^{2+} to disturb long-range ordering of domain by vacancy defect, which would strengthen the relaxor characteristic and expand the stabilized region of the antiferroelectric phase. Sn^{4+} as an equal valence dopant of Ti^{4+} functions not only expands the stabilized region of antiferroelectric, but also adjusts Zr/Ti ratio to enable Ti up to 10 mol%. Currently, the related works of stabilizing the Pb-based antiferroelectric phase mainly focus on adjusting suitable Zr/Sn/Ti ratio [183–185]. Liu *et al*. [186] found that $E_{A–F}$ linearly increased and the squareness of *P*–*E* loop slightly improved when Ti content reduces from 0.11 to 0.07 mol at a fixed Zr of 0.58 mol. W_{rec} enhances, thereby, from 0.28 to 2.35 J/cm^3 for $Pb_{0.97}La_{0.02}(Zr_{0.58}Sn_{0.35}Ti_{0.07})O_3$ antiferroelectric ceramic bulks. In addition, it should be particularly noted that a high W_{rec} is difficult to obtain when $E_{A–F}$ exceeds E_b.

In improving the breakdown behavior of Pb-based antiferroelectric ceramic bulks, Zhang *et al*. [187–189]

did a series of works using some special sintering technology. For instance, Zhang *et al*. [188] reported that $(Pb_{0.87}Ba_{0.1}La_{0.02})(Zr_{0.68}Sn_{0.24}Ti_{0.08})O_3$ (PBLZST) ceramics using hot-press (HP) possessed a high W_{rec} of 3.2 J/cm^3 at E_b = 180 kV/cm due to smaller grain size and well insulation. Considering that special sintering technology requires expensive equipment, this method is not suitable for large-scale production. Some low-cost and convenient solutions are proposed, such as Bian *et al*. [190] used amorphous SiO_2 to coat $Pb_{0.97}La_{0.02}(Zr_{0.33}Sn_{0.55}Ti_{0.12})O_3$ (PLZST 2/33/55/12), and measured a high W_{rec} of 2.68 J/cm^3 due to E_b enhancing from 12.2 to 23.8 kV/mm. It should be noticed that the introduction of non-antiferroelectric phase will reduce the content of the original antiferroelectric phase, even that $E_{A–F}$ would disappear. In a physical method, Wang *et al*. [191] used a rolling process to enhance the mechanical strength of $(Pb_{0.98}La_{0.02})(Zr_{0.55}Sn_{0.45})_{0.995}O_3$ (PLZS) antiferroelectric ceramics. At 400 kV/cm, PLZS ceramics obtain a high W_{rec} of 10.4 J/cm^3 and a η of 87%. Similarly, Zhang *et al*. [192] and Liu *et al*. [193] both utilized tape-casting method to fabricate antiferroelectric thick film. For example, Liu *et al*. [193] utilized tape-casting method to fabricate $(Pb_{0.98-x}La_{0.02}Sr_x)(Zr_{0.9}Sn_{0.1})_{0.995}O_3$ (PLSZS) antiferroelectric thick films, and achieved W_{rec} and η of 11.18 J/cm^3 and 82.2% for x = 0.04, respectively.

Due to the phase structure complexity of PZT-based ceramics near FE–AFE boundary, it usually displays different polarization behavior especially for ceramic films. Gao *et al*. [194] reported different oriented $(Pb_{0.98}La_{0.02})(Zr_{0.95}Ti_{0.05})O_3$ (PLZT) thin films using PLD, obtained a W_{rec} of ~40 J/cm^3 while η only of ~50% for (111) PLZT, which may be related to ferroelectric-like behavior (i.e., high P_r) under high electric field. Despite this condition, the combination of relaxor ferroelectric and antiferroelectric still receives more attention to enhance W_{rec}. In addition, note that antiferroelectric behavior can be observed at different formulas such as PLZT at Zr/Ti ≈ 52:48 [196] or PLZST at Zr/(Sn+Ti) ≈ 65:55 [197]. With the development of micro-electric devices, flexible substrate such as Ti, Si, Ni foils, etc., is required to meet future application scenes. Ma *et al*. [195,198] did a series of meaningful works in the low-cost integration development of PLZT-based thin films. For instance, $Pb_{0.92}La_{0.08}Zr_{0.95}Ti_{0.05}O_3$ (PLZT 8/95/5) antiferroelectric ceramic films possess a high W_{rec} of 53 J/cm^3 at mental foil by CSD, and effective work time would maintain 5000 h at room temperature [195]. Energy storage properties of Pb-based antiferroelectric ceramics and films are summarized and listed in Table 7.

3.3.2 Lead-free antiferroelectric ceramics

(1) $NaNbO_3$

$NaNbO_3$ (NN) is a well-documented nonpolar antiferroelectric phase and possesses a complicated crystal structure due to the rotation of oxygen octahedron

Table 7 Energy storage properties of Pb-based antiferroelectric ceramic bulks and films

Composition	Category	t	W_{rec} (J/cm^3)	η (%)	ε_r @ RT	E_b (kV/cm)	Ref.
PZ	Thin film	300–600 nm	7.1	—	120–200	—	[164]
PSZ5	Thin film	500 nm	14.5	78	~150	900	[165]
α-Fe_2O_3 modified PZ	Thin film	660 nm	17.4	~58	—	600	[169]
PZ:NiO	Thin film	140–170 nm	24.6	~70	~600	1000	[170]
Up-graded Eu-doped PZ	Thin film	400 nm	16.3	67.4	~300	1000	[168]
PLHS	Bulk	0.11 mm	7.63	94	~280	380	[176]
PHO	Thin film	330 nm	24.9	73	—	2957	[177]
PLZST 2/58/35/7	Bulk	0.5 mm	2.35	86.1	~450	120	[186]
PBLZST	Bulk	0.6 mm	3.2	—	—	180	[188]
PLZST 2/33/55/12 @5 mol% SiO_2	Bulk	0.2 mm	2.68	—	~800	238	[190]
PLZS	Bulk	0.11 mm	10.4	87	~180	400	[191]
PLSZS	Thick film	0.1 mm	11.18	82.2	~200	~400	[193]
PLZT 2/95/5	Thin film	300 nm	40	53	—	1000	[194]
PLZT 8/95/5	Thick film	1 μm	53	—	~560	3500	[195]

PZ: $PbZrO_3$; PSZ5: $(Pb_{0.95}Sr_{0.05})ZrO_3$; PLHS: $Pb_{0.98}La_{0.02}(Hf_{0.45}Sn_{55})_{0.995}O_3$; PHO: $PbHfO_3$; PLZST 2/58/35/7: $Pb_{0.97}La_{0.02}(Zr_{0.58}Sn_{0.42-y}Ti_y)O_3$; PBLZST: $(Pb_{0.87}Ba_{0.1}La_{0.02})(Zr_{0.68}Sn_{0.24}Ti_{0.08})O_3$; PLZST 2/33/55/12: $Pb_{0.97}La_{0.02}(Zr_{0.33}Sn_{0.55}Ti_{0.12})O_3$; PLZS: $(Pb_{0.98}La_{0.02})(Zr_{0.55}Sn_{0.45})_{0.995}O_3$; PLSZS: $(Pb_{0.94}La_{0.02}Sr_{0.04})(Zr_{0.9}Sn_{0.1})_{0.995}O_3$; PLZT 2/95/5: $Pb_{0.98}La_{0.02}Zr_{0.95}Ti_{0.05}O_3$; PLZT 8/95/5: $(Pb_{0.92}La_{0.08})(Zr_{0.95}Ti_{0.05})O_3$.

and off-centered displacement of Nb^{5+} [199,200]. In addition to temperature-induced transition, antiferroelectric–ferroelectric phase transition can also be induced by mechanical stress [201], grain size [202], and electric field [203]. Note that an electric field-induced antiferroelectric–ferroelectric phase transition is usually irreversible at room temperature because of the small free energy difference between antiferroelectric and ferroelectric.

Generally, reducing tolerance factor t is still a widely accepted method to stabilize antiferroelectric phase of NN ceramics. For instance, Shimizu *et al*. [204] used $CaZrO_3$ (CZ), with similar electronegativity but smaller tolerance factor t, to modify NN ceramics. As the content of CZ increases, an obvious double P–E loop accompanying to E_{A-F} gradually increases while P_{max} decreases, as shown in Fig. 13. Since then, other compounds such as $SrZrO_3$ (SZ) [205], $CaHfO_3$ (CH) [206], $BiScO_3$ (BS) [207], are both utilized to stabilize antiferroelectric phase, but few reports their energy storage performances. It should be pointed that double P–E loop of NN-based ceramics still has more hysteresis loop at room temperature resulting in low W_{rec}. Moreover, Zhou *et al*. [208] firstly reported Bi_2O_3 modified NN energy storage ceramic bulks, obtained a high W_{rec} of 4.03 J/cm^3 for $Na_{0.7}Bi_{0.1}NbO_3$ ceramics at E_b = 250 kV/cm attributed to the disrupted random electric field and reduced domain size. Energy storage properties of $Na_{0.7}Bi_{0.1}NbO_3$ system show good temperature stability (20–100 ℃), fatigue endurance (10^5 cycles), and charge–discharge properties. After that, more Bi-based compounds including $Bi(Mg_{1/3}Nb_{2/3})O_3$ (BMN) [209], $Bi(Ni_{1/2}Sn_{1/2})O_3$ (BNS) [210], and so on, are used to improve the relaxor characteristics and acquire high W_{rec}. It is particularly important that P–E loop of $BiMeO_3$ modified system becomes slimmer than pure NN ceramic, but characteristic double hysteresis loop fails to be observed.

A double P–E hysteresis loop can be observed in high quality NN single crystal and ceramic film compared with ceramic bulk. However, a few studies reported energy storage properties of NN-based ceramic films, and concentrated on piezoelectric, dielectric tunability. In 2018, Fujii *et al*. [211] deposited $0.92NaNbO_3$–$0.08SrZrO_3$ (0.92NN–0.08SZ) antiferroelectric thin films on $SrRuO_3$ buffered ST substrates with different orientations by using PLD. 0.92NN–0.08SZ thin films with (110) oriented ST substrate exhibit antiferroelectric behavior, while that with (001) oriented substrate is still ferroelectric. Recently, Beppu *et al*. [212] obtained W_{rec} only of 2.9 J/cm^3 for 0.92NN–0.08SZ thin films at $E_b \approx$ 400 kV/cm. In addition, Luo *et al*. [213] fabricated Mn-doped $0.96NaNbO_3$–$0.04CaZrO_3$ (0.96NN–0.04CZ) thin films using sol–gel method, and leakage current of 1 mol% Mn reduces the magnitude of 10^3–10^4 compared to pure compositions. W_{rec} and η of 1 mol% Mn thin films are19.64 J/cm^3 and 64.5%, respectively. Nevertheless, simple composition and no toxic metal elements make it have broad prospects for energy storage research in the future.

(2) $AgNbO_3$

$AgNbO_3$ (AN) has a complicated phase structure and relatively low bandgap (~2.8 eV), and still has difficulty in observing double hysteresis loop at room temperature. Early studies of AN ceramics therefore concentrated on microwave communication and photocatalysis [214,215]. In addition, Ag_2O decomposition

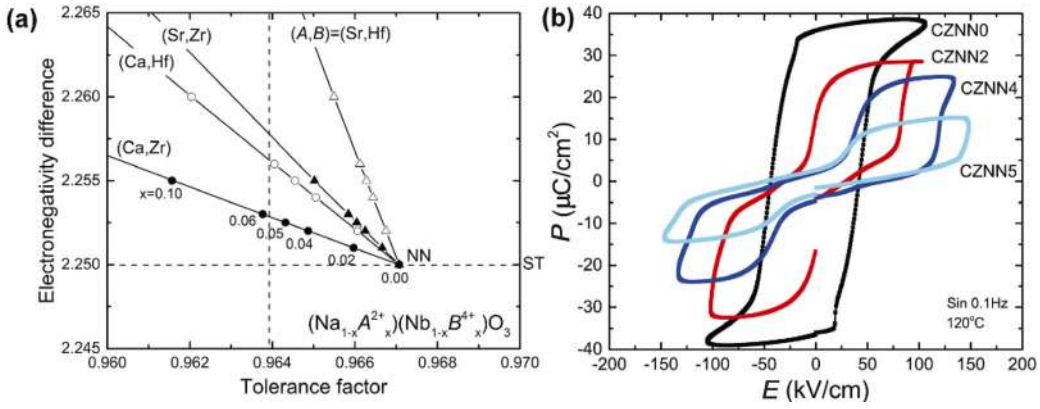

Fig. 13 (a) Tolerance factor versus averaged electronegativity difference for $(Na_{1-x}A_{2+x})(Nb_{1-x}B_{4+x})O_3$ composition, where (A,B) = (Ca,Zr), (Ca,Hf), (Sr,Zr), and (Sr,Hf); (b) P–E loops in the CZNN ceramics at 120 ℃. Reproduced with permission from Ref. [204], © Royal Society of Chemistry 2015.

at a high temperature requires the fabrication of AN-based ceramics at the oxygen-rich environment. Similar to NN, AN-based ceramic bulk is a main research direction for energy storage capacitors.

In 2007, Fu *et al*. [216] successfully fabricated AN ceramics with a double hysteresis loop, and P_{max} can up to 52 μC/cm^2 at 220 kV/cm exceeding other dielectric materials at the same electric field. The phenomenon strongly stimulates the studies of AN ceramics on energy storage applications. Tian *et al*. [217] synthesized pure AN antiferroelectric ceramic bulks, found two polarization structures by TEM and variable temperature *P*–*I*–*E* loops, and attained a high W_{rec} of 2.1 J/cm^3. In general, AN ceramics experience a series phase transition [218]:

$$\text{M1} \xrightarrow{67\,℃} \text{M2} \xrightarrow{267\,℃} \text{M3} \xrightarrow{353\,℃}$$

$$\text{O1} \xrightarrow{361\,℃} \text{O2} \xrightarrow{387\,℃} \text{T} \xrightarrow{579\,℃} \text{C}$$

where M1, M2, and M3 denote orthorhombic phases in rhombic orientation, O1 and O2 are the orthorhombic phases in a parallel orientation, while T and C denote the tetragonal and cubic phases, respectively. It is known that the stability of antiferroelectric phase of AN ceramic is closely related to phase transition among M1, M2, and M3. Therefore, reducing phase transition temperature among M1, M2, and M3 to low temperature would enhance W_{rec} of AN-based ceramics [218–221].

Chemical doping is a simple and effective method to enhance W_{rec} of AN-based ceramic bulks. For example, Ta^{5+} [218,222] and W^{3+} [223] substitute Nb^{5+} of B site, and Bi^{3+} [224], Ca^{2+} [225], and La^{3+} [226] replace Ag^+ of A site. In 2017, Zhao *et al*. [218] fabricated $Ag(Nb_{1-x}Ta_x)O_3$ antiferroelectric ceramics, and P_r decreases from 3.6 to 1.2 μC/cm^2 whereas E_b enhances from 175 to 242 kV/cm with increasing Ta content. $Ag(Nb_{0.85}Ta_{0.15})O_3$ exhibits a high W_{rec} of 4.2 J/cm^3, together with η of 69%, as shown in Figs. 14(a) and 14(b). The authors attribute the enhancement of W_{rec} to the low polarizability of Ta^{5+} because of a closed *t* value. Since then, Zhao *et al*. [223] have done some works to verify the possibility. Besides, electronegativity difference is also playing a crucial role in influencing the function behavior of antiferroelectric materials [227].

Note that fine-grain ceramics is a good choice to enhance E_b due to an inverse relationship between E_b and grain size. Recently, Wang *et al*. [228] synthesized AN ceramics using hydrothermal process, and obtained a maximum E_b = 250 kV/cm among pure AN ceramics so far. However, P_{max} has an obvious decrease compared with other AN ceramics using solid-state method, and thus W_{rec} and η are only of 1.8 J/cm^3 and 40%, respectively. It is noteworthy that little attention has been shared on enhancing E_b of AN ceramics by other different methods apart from ion-doping. Energy storage behaviors of NN and AN antiferroelectric ceramic bulks and films are summarized and listed in Table 8.

In summary, for antiferroelectric ceramics, tolerance factor *t*, electronegative difference, and polarizability are all influencing the stability of antiferroelectric phase. Note that the characteristic double *P*–*E* loop of pure antiferroelectric phase is difficult to be observed, which needs to further explore the related reasons. Physical (special sintering technology, rolling process, etc.) and chemical (coating, hydrothermal process, etc.) methods can enhance E_b by improving sintering behavior or mechanical strength.

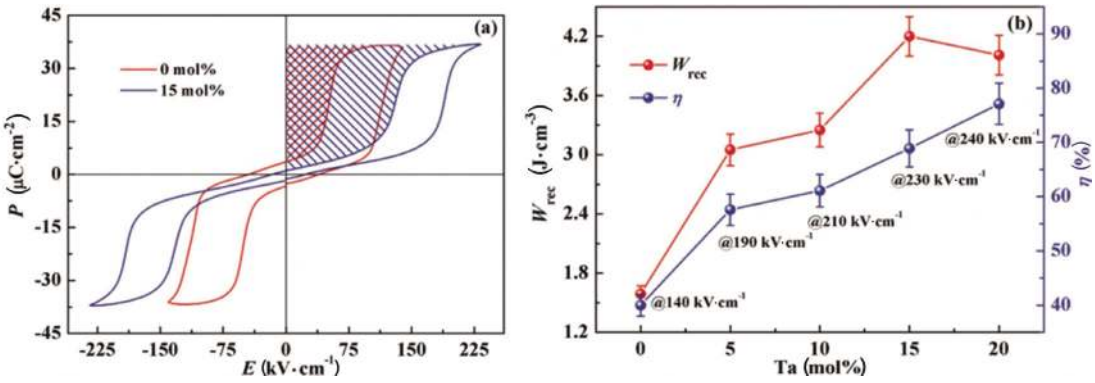

Fig. 14 (a) *P*–*E* loops of $AgNbO_3$ and $Ag(Nb_{0.85}Ta_{0.15})O_3$ ceramic; (b) energy storage performances of $Ag(Nb_{1-x}Ta_x)O_3$ ceramics prior to their breakdown. Reproduced with permission from Ref. [218], © WILEY-VCH Verlag GmbH & Co. KGaA, Weinheim 2017.

Table 8 Energy storage properties of NN and AN-based antiferroelectric ceramic bulks and films

Composition	Category	t	W_{rec} (J/cm^3)	η (%)	ε_r @ RT	E_b (kV/cm)	Ref.
$Na_{0.7}Bi_{0.1}NbO_3$	Bulk	0.2 mm	3.44	85.4	~1700	351	[208]
0.92NN–0.08SZ	Thick film	1 μm	2.9	67	211	400	[212]
1 mol% Mn-doped 0.96NN–0.04CZ	Thin film	300 nm	19.64	64.5	~2200	833.3	[213]
AN	Bulk	0.5 mm	2.1	—	~300	175	[217]
ANT15	Bulk	200 μm	4.2	69	~200	233	[218]
AN	Bulk	150 μm	~1.8	~40	~80	250	[228]

NN: $NaNbO_3$; SZ: $SrZrO_3$; CZ: $CaZrO_3$; AN: $AgNbO_3$; ANT15: $Ag(Nb_{0.85}Ta_{0.15})O_3$.

4 Conclusions and perspectives

From the perspectives of composition modification, structural design, and electrical performance optimization, this paper briefly compares the research progress of energy storage ceramic bulks and films. Currently, W_{rec} of ceramic bulks is generally less than 10 J/cm^3, while that of films can reach 10^2 J/cm^3. Except for ceramic composition, W_{rec} is also closely related to other factors such as sample thickness, preparation, and testing methods. Although giant ε_r linear dielectric attracts more attention, it may be not suitable for energy storage capacitors. In contrast, relaxor ferroelectric and antiferroelectric with high P_{max} and low P_r are easier to obtain high W_{rec} than linear dielectric, so they are relatively ideal energy storage dielectric materials. Whether for bulks or films, E_b is a decisive factor for affecting the upper limit of W_{rec}. In addition, the development from material to device still has a large gap, and thus needs to make more efforts to solve this problem. Judging from the existing researches, the authors believe that the following aspects need further exploration and improvement:

1) It is still a long process to select the ideal energy storage ceramics through a single experiment. If relevant predictions and screenings can be combined with theoretical calculations or machine learning methods, work efficiency will be greatly improved.

2) In order to better understand the variation in domain and phase structures as functions of the electric field, thermal, force, magnetic, etc., external fields, *in-situ* observation technique would be an important direction, which would help us to comprehensively understand the microscopic evolution mechanism of polarization.

3) For materials with crystalline/amorphous phase and multilayer structure, the issues of generation reason and corresponding mechanisms of interface behaviors (such as interface polarization, fatigue, etc.) and stress still need to be deeply investigated.

4) Considering many factors to influence W_{rec} and η, it is important to standardize the test parameters such as sample thickness, area of electrode, testing frequency, and AC/DC conditions, and establish the relevant test standard for performance evaluation of energy storage materials.

Acknowledgements

This work was financially supported by the National Natural Science Foundation of China (51767010).

References

[1] Yang LT, Kong X, Li F, *et al*. Perovskite lead-free dielectrics for energy storage applications. *Prog Mater Sci* 2019, **102**: 72–108.

[2] Yao ZH, Song Z, Hao H, *et al*. Homogeneous/inhomogeneous-structured dielectrics and their energy-storage performances. *Adv Mater* 2017, **29**: 1601727.

[3] Li Q, Han K, Gadinski MR, *et al*. High energy and power density capacitors from solution-processed ternary ferroelectric polymer nanocomposites. *Adv Mater* 2014, **26**: 6244–6249.

[4] Wang Y, Song Y, Xia Y. Electrochemical capacitors: Mechanism, materials, systems, characterization and applications. *Chem Soc Rev* 2016, **45**: 5925–5950.

[5] Bruce PG, Freunberger SA, Hardwick LJ, *et al*. Li–O_2 and Li–S batteries with high energy storage. *Nat Mater* 2012, **11**: 19–29.

[6] Shao Z, Haile SM. A high-performance cathode for the next generation of solid-oxide fuel cells. *Nature* 2004, **431**: 170–173.

[7] Palneedi H, Peddigari M, Hwang GT, *et al*. High-performance dielectric ceramic films for energy storage capacitors: progress and outlook. *Adv Funct Mater* 2018, **28**: 1803665.

[8] Hao X. A review on the dielectric materials for high energy-storage application. *J Adv Dielect* 2013, **3**: 1330001.

[9] Yao FZ, Yuan Q, Wang Q, *et al*. Multiscale structural engineering of dielectric ceramics for energy storage applications: From bulk to thin films. *Nanoscale* 2020, **12**: 17165–17184.

[10] Tong S. Size and temperature effects on dielectric breakdown of ferroelectric films. *J Adv Ceram* 2021, **10**: 181–186.

[11] Zhao P, Wang H, Wu L, *et al*. High-performance relaxor ferroelectric materials for energy storage applications. *Adv Energy Mater* 2019, **9**: 1803048.

[12] Chen X, Zhang H, Cao F, *et al*. Charge–discharge properties of lead zirconate stannate titanate ceramics. *J Appl Phys* 2009, **106**: 034105.

[13] Yang SM, Jo JY, Kim TH, *et al*. AC dynamics of ferroelectric domains from an investigation of the frequency dependence of hysteresis loops. *Phys Rev B* 2010, **82**: 174125.

[14] Huang Y, Li F, Hao H, *et al*. $(Bi_{0.51}Na_{0.47})TiO_3$ based lead free ceramics with high energy density and efficiency. *J Materiomics* 2019, **5**: 385–393.

[15] Li J, Li F, Xu Z, *et al*. Multilayer lead-free ceramic capacitors with ultrahigh energy density and efficiency. *Adv Mater* 2018, **30**: 1802155.

[16] Lou XJ. Polarization fatigue in ferroelectric thin films and related materials. *J Appl Phys* 2009, **105**: 024101.

[17] Ye Y, Zhang SC, Dogan F, *et al*. Influence of nanocrystalline grain size on the breakdown strength of ceramic dielectrics. In: Proceedings of the 14th IEEE International Pulsed Power Conference, 2003: 719–722.

[18] Dervos CT, Thirios, Novacovich J, *et al*. Permittivity properties of thermally treated TiO_2. *Mater Lett* 2004, **58**: 1502–1507.

[19] Reddy CV, Reddy KR, Shetti NP, *et al*. Hetero-nanostructured metal oxide-based hybrid photocatalysts for enhanced photoelectrochemical water splitting—A review. *Int J Hydrog Energy* 2020, **45**: 18331–18347.

[20] Mehta A, Mishra A, Basu S, *et al*. Band gap tuning and surface modification of carbon dots for sustainable environmental remediation and photocatalytic hydrogen production—A review. *J Environ Manag* 2019, **250**: 109486.

[21] Parker R, Wasilik J. Dielectric constant and dielectric loss of TiO_2 (rutile) at low frequencies. *Phys Rev* 1960, **120**: 1631–1637.

[22] Guo D, Ito A, Goto T, *et al*. Preparation of rutile TiO_2 thin films by laser chemical vapor deposition method. *J Adv Ceram* 2013, **2**: 162–166.

[23] Hu W, Liu Y, Withers RL, *et al*. Electron-pinned defect-dipoles for high-performance colossal permittivity materials. *Nat Mater* 2013, **12**: 821–826.

[24] Li J, Li F, Li C, *et al*. Evidences of grain boundary capacitance effect on the colossal dielectric permittivity in (Nb + In) co-doped TiO_2 ceramics. *Sci Rep* 2015, **5**: 8295.

[25] Li J, Li F, Zhuang Y, *et al*. Microstructure and dielectric properties of (Nb + In) co-doped rutile TiO_2 ceramics. *J Appl Phys* 2014, **116**: 074105.

[26] Dong W, Hu W, Berlie A, *et al*. Colossal dielectric behavior of Ga+Nb co-doped rutile TiO_2. *ACS Appl Mater Interfaces* 2015, **7**: 25321–25325.

[27] Nachaithong T, Kidkhunthod P, Thongbai P, *et al*. Surface barrier layer effect in (In + Nb) co-doped TiO_2 ceramics: An alternative route to design low dielectric loss. *J Am Ceram Soc* 2017, **100**: 1452–1459.

[28] Petzelt J, Nuzhnyy D, Bovtun V, *et al*. Origin of the colossal permittivity of (Nb + In) co-doped rutile ceramics by wide-range dielectric spectroscopy. *Phase Transitions* 2018, **91**: 932–941.

[29] Chao S, Petrovsky V, Dogan F. Effects of sintering temperature on the microstructure and dielectric properties of titanium dioxide ceramics. *J Mater Sci* 2010, **45**: 6685–6693.

[30] Liu J, Zhang J, Wei M, *et al*. Dielectric properties of manganese-doped TiO_2 with different alkali-free glass contents for energy storage application. *J Mater Sci*: *Mater Electron* 2016, **27**: 7680–7684.

[31] Chao S, Dogan F. Processing and dielectric properties of TiO_2 thick films for high-energy density capacitor applications. *Int J Appl Ceram Technol* 2011, **8**: 1363–1373.

[32] Pai YY, Tylan-Tyler A, Irvin P, *et al*. Physics of $SrTiO_3$-based heterostructures and nanostructures: A review. *Rep Prog Phys* 2018, **81**: 036503.

[33] Kumar Yadav A, Gautam CR. A review on crystallisation behaviour of perovskite glass ceramics. *Adv Appl Ceram* 2014, **113**: 193–207.

[34] Hu QG, Shen ZY, Li YM, *et al*. Enhanced energy storage properties of dysprosium doped strontium titanate ceramics. *Ceram Int* 2014, **40**: 2529–2534.

[35] Kong X, Yang L, Cheng Z, *et al*. Bi-modified $SrTiO_3$-based ceramics for high-temperature energy storage applications. *J Am Ceram Soc* 2020, **103**: 1722–1731.

[36] Fergus JW. Oxide materials for high temperature thermoelectric energy conversion. *J Eur Ceram Soc* 2012, **32**: 525–540.

[37] Wang Y, Shen ZY, Li YM, *et al*. Optimization of energy storage density and efficiency in $Ba_xSr_{1-x}TiO_3$ ($x \leq 0.4$) paraelectric ceramics. *Ceram Int* 2015, **41**: 8252–8256.

[38] Nishigaki S, Murano K, Ohkoshi A. Dielectric properties of ceramics in the system $(Sr_{0.50}Pb_{0.25}Ca_{0.25})TiO_3$–$Bi_2O_3{\cdot}3TiO_2$ and their applications in a high-voltage capacitor. *J Am Ceram Soc* 1982, **65**: 554–560.

[39] Kong X, Yang L, Cheng Z, *et al*. $(Ba,Sr)TiO_3$–$Bi(Mg,Hf)O_3$ lead-free ceramic capacitors with high energy density and energy efficiency. *ACS Appl Energy Mater* 2020, **3**: 12254–12262.

[40] Fletcher NH, Hilton AD, Ricketts BW. Optimization of energy storage density in ceramic capacitors. *J Phys D*: *Appl Phys* 1996, **29**: 253–258.

[41] Ang C, Yu Z, Cross LE. Oxygen-vacancy-related low-frequency dielectric relaxation and electrical

conduction in Bi: $SrTiO_3$. *Phys Rev B* 2000, **62**: 228–236.
[42] Yu Z, Ang C. Dielectric relaxor and ferroelectric relaxor: Bi-doped paraelectric $SrTiO_3$. *J Appl Phys* 2002, **91**: 1487–1494.
[43] Yu Z, Ang C. High capacitance-temperature sensitivity and "giant" dielectric constant in $SrTiO_3$. *Appl Phys Lett* 2007, **90**: 202903.
[44] Shen ZY, Hu QG, Li YM, *et al*. Structure and dielectric properties of $Re_{0.02}Sr_{0.97}TiO_3$ (Re = La, Sm, Gd, Er) ceramics for high-voltage capacitor applications. *J Am Ceram Soc* 2013, **96**: 2551–2555.
[45] Shen ZY, Li YM, Luo WQ, *et al*. Structure and dielectric properties of $Nd_xSr_{1-x}TiO_3$ ceramics for energy storage application. *J Mater Sci*: *Mater Electron* 2013, **24**: 704–710.
[46] Shen ZY, Luo WQ, Li YM, *et al*. Electrical hetero-structure of $Nd_{0.1}Sr_{0.9}TiO_3$ ceramic for energy storage applications. *J Mater Sci*: *Mater Electron* 2013, **24**: 607–612.
[47] Song Z, Liu H, Zhang S, *et al*. Effect of grain size on the energy storage properties of $(Ba_{0.4}Sr_{0.6})TiO_3$ paraelectric ceramics. *J Eur Ceram Soc* 2014, **34**: 1209–1217.
[48] Wu YJ, Huang YH, Wang N, *et al*. Effects of phase constitution and microstructure on energy storage properties of barium strontium titanate ceramics. *J Eur Ceram Soc* 2017, **37**: 2099–2104.
[49] Zhang Q, Wang L, Luo J, *et al*. Improved energy storage density in barium strontium titanate by addition of $BaO–SiO_2–B_2O_3$ glass. *J Am Ceram Soc* 2009, **92**: 1871–1873.
[50] Kim SH, Koh JH. ZnBO-doped $(Ba,Sr)TiO_3$ ceramics for the low-temperature sintering process. *J Eur Ceram Soc* 2008, **28**: 2969–2973.
[51] Shen ZY, Wang Y, Tang YX, *et al*. Glass modified Barium strontium titanate ceramics for energy storage capacitor at elevated temperatures. *J Materiomics* 2019, **5**: 641–648.
[52] Yang X, Li W, Qiao Y, *et al*. High energy-storage density of lead-free $(Sr_{1-1.5x}Bi_x)Ti_0{\cdot}99Mn_{0.01}O_3$ thin films induced by Bi^{3+}-VSr dipolar defects. *Phys Chem Chem Phys* 2019, **21**: 16359–16366.
[53] Zhang Y, Li W, Wang Z, *et al*. Ultrahigh energy storage and electrocaloric performance achieved in $SrTiO_3$ amorphous thin films via polar cluster engineering. *J Mater Chem A* 2019, **7**: 17797–17805.
[54] Pan H, Zeng Y, Shen Y, *et al*. $BiFeO_3–SrTiO_3$ thin film as a new lead-free relaxor-ferroelectric capacitor with ultrahigh energy storage performance. *J Mater Chem A* 2017, **5**: 5920–5926.
[55] Hou C, Huang W, Zhao W, *et al*. Ultrahigh energy density in $SrTiO_3$ film capacitors. *ACS Appl Mater Interfaces* 2017, **9**: 20484–20490.
[56] Gao W, Yao M, Yao X. Improvement of energy density in $SrTiO_3$ film capacitor via self-repairing behavior. *Ceram Int* 2017, **43**: 13069–13074.
[57] Gao W, Yao M, Yao X. Achieving ultrahigh breakdown strength and energy storage performance through periodic interface modification in $SrTiO_3$ thin film. *ACS Appl Mater Interfaces* 2018, **10**: 28745–28753.
[58] Chen X, Peng B, Ding M, *et al*. Giant energy storage density in lead-free dielectric thin films deposited on Si wafers with an artificial dead-layer. *Nano Energy* 2020, **78**: 105390.
[59] Cross LE. Relaxor ferroelectrics. *Ferroelectrics* 1987, **76**: 241–267.
[60] Pan Z, Wang P, Hou X, *et al*. Fatigue-free aurivillius phase ferroelectric thin films with ultrahigh energy storage performance. *Adv Energy Mater* 2020, **10**: 2001536.
[61] Shrout TR, Zhang SJ. Lead-free piezoelectric ceramics: Alternatives for PZT? *J Electroceramics* 2007, **19**: 113–126.
[62] Jaffe B, Cook WR, Jaffe H. *Piezoelectric Ceramics Academic*. Amsterdam: Elsevier, 1971.
[63] Chen Y, Wang S, Zhou H, *et al*. A systematic analysis of the radial resonance frequency spectra of the PZT-based (Zr/Ti = 52/48) piezoceramic thin disks. *J Adv Ceram* 2020, **9**: 380–392.
[64] Gao J, Liu Y, Wang Y, *et al*. High temperature-stability of $(Pb_{0.9}La_{0.1})(Zr_{0.65}Ti_{0.35})O_3$ ceramic for energy-storage applications at finite electric field strength. *Scripta Mater* 2017, **137**: 114–118.
[65] Zhang TF, Tang XG, Liu QX, *et al*. Energy-storage properties and high-temperature dielectric relaxation behaviors of relaxor ferroelectric $Pb(Mg_{1/3}Nb_{2/3})O_3–PbTiO_3$ ceramics. *J Phys D*: *Appl Phys* 2016, **49**: 095302.
[66] Kumar A, Kim SH, Peddigari M, *et al*. High energy storage properties and electrical field stability of energy efficiency of $(Pb_{0.89}La_{0.11})(Zr_{0.70}Ti_{0.30})_{0.9725}O_3$ relaxor ferroelectric ceramics. *Electron Mater Lett* 2019, **15**: 323–330.
[67] Zhang T, Li W, Hou Y, *et al*. High-energy storage density and excellent temperature stability in antiferroelectric/ferroelectric bilayer thin films. *J Am Ceram Soc* 2017, **100**: 3080–3087.
[68] Zhang T, Li W, Zhao Y, *et al*. High energy storage performance of opposite double-heterojunction ferroelectricity-insulators. *Adv Funct Mater* 2018, **28**: 1706211.
[69] Ma B, Hu Z, Koritala RE, *et al*. PLZT film capacitors for power electronics and energy storage applications. *J Mater Sci*: *Mater Electron* 2015, **26**: 9279–9287.
[70] Peng B, Tang S, Lu L, *et al*. Low-temperature-poling awakened high dielectric breakdown strength and outstanding improvement of discharge energy density of $(Pb,La)(Zr,Sn,Ti)O_3$ relaxor thin film. *Nano Energy* 2020, **77**: 105132.
[71] Dai X, Viehland D. Effects of lanthanum modification on the antiferroelectric-ferroelectric stability of high zirconium-content lead zirconate titanate. *J Appl Phys* 1994, **76**: 3701–3709.
[72] Gupta SM, Li JF, Viehland D. Coexistence of relaxor and normal ferroelectric phases in morphotropic phase

boundary compositions of lanthanum-modified lead zirconate titanate. *J Am Ceram Soc* 1998, **81**: 557–564.

[73] Hu Z, Ma B, Liu S, *et al*. Relaxor behavior and energy storage performance of ferroelectric PLZT thin films with different Zr/Ti ratios. *Ceram Int* 2014, **40**: 557–562.

[74] Liu Y, Hao X, An S. Significant enhancement of energy-storage performance of $(Pb_{0.91}La_{0.09})(Zr_{0.65}Ti_{0.35})O_3$ relaxor ferroelectric thin films by Mn doping. *J Appl Phys* 2013, **114**: 174102.

[75] Peng B, Xie Z, Yue Z, *et al*. Improvement of the recoverable energy storage density and efficiency by utilizing the linear dielectric response in ferroelectric capacitors. *Appl Phys Lett* 2014, **105**: 052904.

[76] Zhang L, Hao X, Yang J, *et al*. Large enhancement of energy-storage properties of compositional graded $(Pb_{1-x}La_x)(Zr_{0.65}Ti_{0.35})O_3$ relaxor ferroelectric thick films. *Appl Phys Lett* 2013, **103**: 113902.

[77] Nguyen MD, Houwman EP, Rijnders G. Energy storage performance and electric breakdown field of thin relaxor ferroelectric PLZT films using microstructure and growth orientation control. *J Phys Chem C* 2018, **122**: 15171–15179.

[78] Nguyen MD, Nguyen CTQ, Vu HN, *et al*. Controlling microstructure and film growth of relaxor-ferroelectric thin films for high break-down strength and energy-storage performance. *J Eur Ceram Soc* 2018, **38**: 95–103.

[79] Smolenskii GA, Isupov VA, Agranovskaya AI, *et al*. New ferroelectrics of complex composition IV. *J Sov Phy Solid State* 1961, **2**: 2651–2654.

[80] Rao BN, Datta R, Chandrashekaran SS, *et al*. Local structural disorder and its influence on the average global structure and polar properties in $Na_{0.5}Bi_{0.5}TiO_3$. *Phys Rev B* 2013, **88**: 224103.

[81] Reichmann K, Feteira A, Li M. Bismuth sodium titanate based materials for piezoelectric actuators. *Materials* 2015, **8**: 8467–8495.

[82] Suchanicz J, Kluczewska-Chmielarz K, Sitko D, *et al*. Electrical transport in lead-free $Na_{0.5}Bi_{0.5}TiO_3$ ceramics. *J Adv Ceram* 2021, **10**: 152–165.

[83] Qiao X, Zhang F, Wu D, *et al*. Superior comprehensive energy storage properties in $Bi_{0.5}Na_{0.5}TiO_3$-based relaxor ferroelectric ceramics. *Chem Eng J* 2020, **388**: 124158.

[84] Yang F, Pan Z, Ling Z, *et al*. Realizing high comprehensive energy storage performances of BNT-based ceramics for application in pulse power capacitors. *J Eur Ceram Soc* 2021, **41**: 2548–2558.

[85] Zhang X, Hu D, Pan Z, *et al*. Enhancement of recoverable energy density and efficiency of lead-free relaxor-ferroelectric BNT-based ceramics. *Chem Eng J* 2021, **406**: 126818.

[86] Zhu C, Cai Z, Luo B, *et al*. High temperature lead-free BNT-based ceramics with stable energy storage and dielectric properties. *J Mater Chem A* 2020, **8**: 683–692.

[87] Ma C, Tan X. *In situ* transmission electron microscopy study on the phase transitionsin lead-free $(1-x)(Bi_{1/2}Na_{1/2})TiO_3$–$xBaTiO_3$ ceramics. *J Am Ceram Soc* 2011, **94**: 4040–4044.

[88] Jo W, Schaab S, Sapper E, *et al*. On the phase identity and its thermal evolution of lead free $(Bi_{1/2}Na_{1/2})TiO_3$–6 mol% $BaTiO_3$. *J Appl Phys* 2011, **110**: 074106.

[89] Ye H, Yang F, Pan Z, *et al*. Significantly improvement of comprehensive energy storage performances with lead-free relaxor ferroelectric ceramics for high-temperature capacitors applications. *Acta Mater* 2021, **203**: 116484.

[90] Gao F, Dong X, Mao C, *et al*. Energy-storage properties of $0.89Bi_{0.5}Na_{0.5}TiO_3$–$0.06BaTiO_3$–$0.05K_{0.5}Na_{0.5}NbO_3$ lead-free anti-ferroelectric ceramics. *J Am Ceram Soc* 2011, **94**: 4382–4386.

[91] Cao W, Li W, Feng Y, *et al*. Defect dipole induced large recoverable strain and high energy-storage density in lead-free $Na_{0.5}Bi_{0.5}TiO_3$-based systems. *Appl Phys Lett* 2016, **108**: 202902.

[92] Ren X. Large electric-field-induced strain in ferroelectric crystals by point-defect-mediated reversible domain switching. *Nat Mater* 2004, **3**: 91–94.

[93] Li F, Zhai J, Shen B, *et al*. Influence of structural evolution on energy storage properties in $Bi_{0.5}Na_{0.5}TiO_3$–$SrTiO_3$–$NaNbO_3$ lead-free ferroelectric ceramics. *J Appl Phys* 2017, **121**: 054103.

[94] Yang L, Kong X, Cheng Z, *et al*. Ultra-high energy storage performance with mitigated polarization saturation in lead-free relaxors. *J Mater Chem A* 2019, **7**: 8573–8580.

[95] Li D, Shen ZY, Li ZP, *et al*. *P*–*E* hysteresis loop going slim in $Ba_{0.3}Sr_{0.7}TiO_3$-modified $Bi_{0.5}Na_{0.5}TiO_3$ ceramics for energy storage applications. *J Adv Ceram* 2020, **9**: 183–192.

[96] Li D, Shen Z-Y, Li Z, *et al*. Optimization of polarization behavior in $(1-x)$BSBNT–xNN ceramics for pulsed power capacitors. *J Mater Chem C* 2020, **8**: 7650–7657.

[97] Li J, Shen Z, Chen X, *et al*. Grain-orientation-engineered multilayer ceramic capacitors for energy storage applications. *Nat Mater* 2020, **19**: 999–1005.

[98] Yang H, Liu P, Yan F, *et al*. A novel lead-free ceramic with layered structure for high energy storage applications. *J Alloys Compd* 2019, **773**: 244–249.

[99] Jia W, Hou Y, Zheng M, *et al*. Superior temperature-stable dielectrics for MLCCs based on $Bi_{0.5}Na_{0.5}TiO_3$–$NaNbO_3$ system modified by $CaZrO_3$. *J Am Ceram Soc* 2018, **101**: 3468–3479.

[100] Wang H, Zhao P, Chen L, *et al*. Energy storage properties of $0.87BaTiO_3$–$0.13Bi(Zn_{2/3}(Nb_{0.85}Ta_{0.15})_{1/3})O_3$ multilayer ceramic capacitors with thin dielectric layers. *J Adv Ceram* 2020, **9**: 292–302.

[101] Feng C, Yang CH, Li SX, *et al*. Reduced leakage current and large polarization of $Na_{0.5}Bi_{0.5}Ti_{0.98}Mn_{0.02}O_3$ thin film annealed at low temperature. *Ceram Int* 2015, **41**: 14179–14183.

[102] Wang J, Sun N, Li Y, *et al*. Effects of Mn doping on dielectric properties and energy-storage performance of $Na_{0.5}Bi_{0.5}TiO_3$ thick films. *Ceram Int* 2017, **43**:

7804–7809.

[103] Feng C, Yang CH, Sui HT, *et al*. Effect of Fe doping on the crystallization and electrical properties of $Na_{0.5}Bi_{0.5}TiO_3$ thin film. *Ceram Int* 2015, **41**: 4214–4217.

[104] Zhang YL, Li WL, Cao WP, *et al*. Enhanced energy-storage performance of 0.94NBT–0.06BT thin films induced by a $Pb_{0.8}La_{0.1}Ca_{0.1}Ti_{0.975}O_3$ seed layer. *Ceram Int* 2016, **42**: 14788–14792.

[105] Peng B, Zhang Q, Li X, *et al*. Giant electric energy density in epitaxial lead-free thin films with coexistence of ferroelectrics and antiferroelectrics. *Adv Electron Mater* 2015, **1**: 1500052.

[106] Chen P, Wu S, Li P, *et al*. Great enhancement of energy storage density and power density in BNBT/*x*BFO multilayer thin film hetero-structures. *Inorg Chem Front* 2018, **5**: 2300–2305.

[107] Qian J, Han Y, Yang C, *et al*. Energy storage performance of flexible NKBT/NKBT–ST multilayer film capacitor by interface engineering. *Nano Energy* 2020, **74**: 104862.

[108] Guo Y, Li M, Zhao W, *et al*. Ferroelectric and pyroelectric properties of $(Na_{0.5}Bi_{0.5})TiO_3$–$BaTiO_3$ based trilayered thin films. *Thin Solid Films* 2009, **517**: 2974–2978.

[109] Pan MJ, Randall CA. A brief introduction to ceramic capacitors. *IEEE Electr Insul Mag* 2010, **26**: 44–50.

[110] Zheng L, Yuan L, Liang G, *et al*. An *in situ* $(K_{0.5}Na_{0.5})NbO_3$-doped Barium titanate foam framework and its cyanate ester resin composites with temperature-stable dielectric properties and low dielectric loss. *Mater Chem Front* 2019, **3**: 726–736.

[111] Acosta M, Novak N, Rojas V, *et al*. $BaTiO_3$-based piezoelectrics: Fundamentals, current status, and perspectives. *Appl Phys Rev* 2017, **4**: 041305.

[112] Gao WX, Zhu Y, Wang YJ, *et al*. A review of flexible perovskite oxide ferroelectric films and their application. *J Materiomics* 2020, **6**: 1–16.

[113] Zheng H, Wang J, Lofland SE, *et al*. Multiferroic $BaTiO_3$–$CoFe_2O_4$ nanostructures. *Science* 2004, **303**: 661–663.

[114] Hu D, Pan Z, Tan X, *et al*. Optimization the energy density and efficiency of $BaTiO_3$-based ceramics for capacitor applications. *Chem Eng J* 2021, **409**: 127375.

[115] Ogihara H, Randall CA, Trolier-Mckinstry S. High-energy density capacitors utilizing $0.7BaTiO_3$–$0.3BiScO_3$ ceramics. *J Am Ceram Soc* 2009, **92**: 1719–1724.

[116] Wu L, Wang X, Li L. Core–shell $BaTiO_3$@$BiScO_3$ particles for local graded dielectric ceramics with enhanced temperature stability and energy storage capability. *J Alloys Compd* 2016, **688**: 113–121.

[117] Yuan Q, Li G, Yao F, *et al*. Simultaneously achieved temperature-insensitive high energy density and efficiency in domain engineered $BaTiO_3$–$Bi(Mg_{0.5}Zr_{0.5})O_3$ lead-free relaxor ferroelectrics. *Nano Energy* 2018, **52**: 203–210.

[118] Choi DH, Baker A, Lanagan M, *et al*. Structural and dielectric properties in $(1-x)BaTiO_3$–$xBi(Mg_{1/2}Ti_{1/2})O_3$ ceramics ($0.1 \leqslant x \leqslant 0.5$) and potential for high-voltage multilayer capacitors. *J Am Ceram Soc* 2013, **96**: 2197–2202.

[119] Li MD, Tang XG, Zeng SM, *et al*. Oxygen-vacancy-related dielectric relaxation behaviours and impedance spectroscopy of $Bi(Mg_{1/2}Ti_{1/2})O_3$ modified $BaTiO_3$ ferroelectric ceramics. *J Materiomics* 2018, **4**: 194–201.

[120] Hanani Z, Mezzane D, Amjoud M, *et al*. Phase transitions, energy storage performances and electrocaloric effect of the lead-free $Ba_{0.85}Ca_{0.15}Zr_{0.10}Ti_{0.90}O_3$ ceramic relaxor. *J Mater Sci*: *Mater Electron* 2019, **30**: 6430–6438.

[121] Wang XW, Zhang BH, Shi YC, *et al*. Enhanced energy storage properties in $Ba_{0.85}Ca_{0.15}Zr_{0.1}Ti_{0.9}O_3$ ceramics with glass additives. *J Appl Phys* 2020, **127**: 074103.

[122] Hanani Z, Merselmiz S, Danine A, *et al*. Enhanced dielectric and electrocaloric properties in lead-free rod-like BCZT ceramics. *J Adv Ceram* 2020, **9**: 210–219.

[123] Patel S, Sharma D, Singh A, *et al*. Enhanced thermal energy conversion and dynamic hysteresis behavior of Sr-added $Ba_{0.85}Ca_{0.15}Ti_{0.9}Zr_{0.1}O_3$ ferroelectric ceramics. *J Materiomics* 2016, **2**: 75–86.

[124] Su X, Riggs BC, Tomozawa M, *et al*. Preparation of $BaTiO_3$/low melting glass core–shell nanoparticles for energy storage capacitor applications. *J Mater Chem A* 2014, **2**: 18087–18096.

[125] Zhang Y, Cao M, Yao Z, *et al*. Effects of silica coating on the microstructures and energy storage properties of $BaTiO_3$ ceramics. *Mater Res Bull* 2015, **67**: 70–76.

[126] Wu L, Wang X, Gong H, *et al*. Core-satellite $BaTiO_3$@$SrTiO_3$ assemblies for a local compositionally graded relaxor ferroelectric capacitor with enhanced energy storage density and high energy efficiency. *J Mater Chem C* 2015, **3**: 750–758.

[127] Cheng H, Ouyang J, Zhang YX, *et al*. Demonstration of ultra-high recyclable energy densities in domain-engineered ferroelectric films. *Nat Commun* 2017, **8**: 1999.

[128] Yu Z, Ang C, Guo RY, *et al*. Ferroelectric-relaxor behavior of $Ba(Ti_{0.7}Zr_{0.3})O_3$ ceramics. *J Appl Phys* 2002, **92**: 2655–2657.

[129] Hennings D, Schnell A, Simon G. Diffuse ferroelectric phase transitions in $Ba(Ti_{1-y}Zry)O_3$ ceramics. *J Am Ceram Soc* 1982, **65**: 539–544.

[130] Instan AA, Pavunny SP, Bhattarai MK, *et al*. Ultrahigh capacitive energy storage in highly oriented $Ba(Zr_xTi_{1-x})O_3$ thin films prepared by pulsed laser deposition. *Appl Phys Lett* 2017, **111**: 142903.

[131] Reddy SR, Prasad VVB, Bysakh S, *et al*. Superior energy storage performance and fatigue resistance in ferroelectric BCZT thin films grown in an oxygen-rich atmosphere. *J Mater Chem C* 2019, **7**: 7073–7082.

[132] Ortega N, Kumar A, Scott JF, *et al*. Relaxor-ferroelectric superlattices: High energy density capacitors. *J Phys*: *Condens Matter* 2012, **24**: 445901.

[133] Sun Z, Ma C, Liu M, *et al*. Ultrahigh energy storage performance of lead-free oxide multilayer film capacitors via interface engineering. *Adv Mater* 2017, **29**: 1604427.

[134] Zhang W, Gao Y, Kang L, *et al*. Space-charge dominated epitaxial $BaTiO_3$ heterostructures. *Acta Mater* 2015, **85**: 207–215.

[135] Ru J, Min D, Lanagan M, *et al*. Enhanced energy storage properties of thermostable sandwich-structured $BaTiO_3$/polyimide nanocomposites with better controlled interfaces. *Mater Des* 2021, **197**: 109270.

[136] Rojac T, Bencan A, Malic B, *et al*. $BiFeO_3$ ceramics: Processing, electrical, and electromechanical properties. *J Am Ceram Soc* 2014, **97**: 1993–2011.

[137] Yang CH, Qian J, Lv P, *et al*. Flexible lead-free BFO-based dielectric capacitor with large energy density, superior thermal stability, and reliable bending endurance. *J Materiomics* 2020, **6**: 200–208.

[138] Gao X, Li Y, Chen J, *et al*. High energy storage performances of $Bi_{1-x}Sm_xFe_{0.95}Sc_{0.05}O_3$ lead-free ceramics synthesized by rapid hot press sintering. *J Eur Ceram Soc* 2019, **39**: 2331–2338.

[139] Yin L, Mi W. Progress in $BiFeO_3$-based heterostructures: Materials, properties and applications. *Nanoscale* 2020, **12**: 477–523.

[140] Li Q, Ji S, Wang D, *et al*. Simultaneously enhanced energy storage density and efficiency in novel $BiFeO_3$-based lead-free ceramic capacitors. *J Eur Ceram Soc* 2021, **41**: 387–393.

[141] Lee MH, Kim DJ, Park JS, *et al*. High-performance lead-free piezoceramics with high curie temperatures. *Adv Mater* 2015, **27**: 6976–6982.

[142] Wu J, Fan Z, Xiao D, *et al*. Multiferroic bismuth ferrite-based materials for multifunctional applications: Ceramic bulks, thin films and nanostructures. *Prog Mater Sci* 2016, **84**: 335–402.

[143] Hang Q, Zhou W, Zhu X, *et al*. Structural, spectroscopic, and dielectric characterizations of Mn-doped $0.67BiFeO_3$–$0.33BaTiO_3$ multiferroic ceramics. *J Adv Ceram* 2013, **2**: 252–259.

[144] Liu N, Liang R, Zhou Z, *et al*. Designing lead-free bismuth ferrite-based ceramics learning from relaxor ferroelectric behavior for simultaneous high energy density and efficiency under low electric field. *J Mater Chem C* 2018, **6**: 10211–10217.

[145] Qi H, Xie A, Tian A, *et al*. Superior energy-storage capacitors with simultaneously giant energy density and efficiency using nanodomain engineered $BiFeO_3$–$BaTiO_3$–$NaNbO_3$ lead-free bulk ferroelectrics. *Adv Energy Mater* 2020, **10**: 1903338.

[146] Wang G, Li J, Zhang X, *et al*. Ultrahigh energy storage density lead-free multilayers by controlled electrical homogeneity. *Energy Environ Sci* 2019, **12**: 582–588.

[147] Correia TM, McMillen M, Rokosz MK, *et al*. A lead-free and high-energy density ceramic for energy storage applications. *J Am Ceram Soc* 2013, **96**: 2699–2702.

[148] Pan H, Li F, Liu Y, *et al*. Ultrahigh-energy density lead-free dielectric films via polymorphic nanodomain design. *Science* 2019, **365**: 578–582.

[149] Kan D, Pálová L, Anbusathaiah V, *et al*. Universal behavior and electric-field-induced structural transition in rare-earth-substituted $BiFeO_3$. *Adv Funct Mater* 2010, **20**: 1108–1115.

[150] McMillen M, Douglas AM, Correia TM, *et al*. Increasing recoverable energy storage in electroceramic capacitors using “dead-layer” engineering. *Appl Phys Lett* 2012, **101**: 242909.

[151] Hou Y, Han R, Li W, *et al*. Significantly enhanced energy storage performance in $BiFeO_3$/$BaTiO_3$/$BiFeO_3$ sandwich-structured films through crystallinity regulation. *Phys Chem Chem Phys* 2018, **20**: 21917–21924.

[152] Zhu H, Liu M, Zhang Y, *et al*. Increasing energy storage capabilities of space-charge dominated ferroelectric thin films using interlayer coupling. *Acta Mater* 2017, **122**: 252–258.

[153] Li JF, Wang K, Zhu FY, *et al*. (K,Na)NbO_3-based lead-free piezoceramics: Fundamental aspects, processing technologies, and remaining challenges. *J Am Ceram Soc* 2013, **96**: 3677–3696.

[154] Egerton L, Dillon DM. Piezoelectric and dielectric properties of ceramics in the system potassium–sodium niobate. *J Am Ceram Soc* 1959, **42**: 438–442

[155] Yang Z, Du H, Qu S, *et al*. Significantly enhanced recoverable energy storage density in potassium–sodium niobate-based lead free ceramics. *J Mater Chem A* 2016, **4**: 13778–13785.

[156] Shao T, Du H, Ma H, *et al*. Potassium-sodium niobate based lead-free ceramics: novel electrical energy storage materials. *J Mater Chem A* 2017, **5**: 554–563.

[157] Qu B, Du H, Yang Z, *et al*. Large recoverable energy storage density and low sintering temperature in potassium-sodium niobate-based ceramics for multilayer pulsed power capacitors. *J Am Ceram Soc* 2017, **100**: 1517–1526.

[158] Qu B, Du H, Yang Z, *et al*. Enhanced dielectric breakdown strength and energy storage density in lead-free relaxor ferroelectric ceramics prepared using transition liquid phase sintering. *RSC Adv* 2016, **6**: 34381–34389.

[159] Yang Y, Ji Y, Fang M, *et al*. Morphotropic relaxor boundary in a relaxor system showing enhancement of electrostrain and dielectric permittivity. *Phys Rev Lett* 2019, **123**: 137601.

[160] Won SS, Kawahara M, Kuhn L, *et al*. $BiFeO_3$-doped $(K_{0.5},Na_{0.5})(Mn_{0.005},Nb_{0.995})O_3$ ferroelectric thin film capacitors for high energy density storage applications. *Appl Phys Lett* 2017, **110**: 152901.

[161] Huang Y, Shu L, Zhang SW, *et al*. Simultaneously achieved high-energy storage density and efficiency in (K,Na)NbO_3-based lead-free ferroelectric films. *J Am Ceram Soc* 2021, **104**: 4119–4130.

[162] Kittel C. Theory of antiferroelectric crystals. *Phys Rev* 1951, **82**: 729–732.

[163] Tagantsev A, Vaideeswaran K, Vakhrushev S, *et al*. The origin of antiferroelectricity in $PbZrO_3$. *Nat Commun* 2013,

4: 2229.

[164] Chen N, Bai G, Auciello O, *et al*. Properties and orientation of antiferroelectric lead zirconate thin films grown by MOCVD. *MRS Online Proc Libr* 1998, **541**: 345–350.

[165] Hao X, Zhai J, Yao X. Improved energy storage performance and fatigue endurance of Sr-doped $PbZrO_3$ antiferroelectric thin films. *J Am Ceram Soc* 2009, **92**: 1133–1135.

[166] Parui J, Krupanidhi SB. Enhancement of charge and energy storage in sol–gel derived pure and La-modified $PbZrO_3$ thin films. *Appl Phys Lett* 2008, **92**: 192901.

[167] Tani T, Li JF, Viehland D, *et al*. Antiferroelectric-ferroelectric switching and induced strains for sol–gel derived lead zirconate thin layers. *J Appl Phys* 1994, **75**: 3017–3023.

[168] Ye M, Sun Q, Chen X, *et al*. Electrical and energy storage performance of Eu-doped $PbZrO_3$ thin films with different gradient sequences. *J Am Ceram Soc* 2012, **95**: 1486–1488.

[169] Sa T, Cao Z, Wang Y, *et al*. Enhancement of charge and energy storage in $PbZrO_3$ thin films by local field engineering. *Appl Phys Lett* 2014, **105**: 043902.

[170] Chen MJ, Ning XK, Wang SF, *et al*. Significant enhancement of energy storage density and polarization in self-assembled $PbZrO_3$:NiO nano-columnar composite films. *Nanoscale* 2019, **11**: 1914–1920.

[171] Ge J, Remiens D, Costecalde J, *et al*. Effect of residual stress on energy storage property in $PbZrO_3$ antiferroelectric thin films with different orientations. *Appl Phys Lett* 2013, **103**: 162903.

[172] Ge J, Remiens D, Dong X, *et al*. Enhancement of energy storage in epitaxial $PbZrO_3$ antiferroelectric films using strain engineering. *Appl Phys Lett* 2014, **105**: 112908.

[173] Corker DL, Glazer AM, Kaminsky W, *et al*. Investigation into the crystal structure of the perovskite lead hafnate, $PbHfO_3$. *Acta Crystallogr Sect B* 1998, **54**: 18–28.

[174] Madigout V, Baudour JL, Bouree F, *et al*. Crystallographic structure of lead hafnate ($PbHfO_3$) from neutron powder diffraction and electron microscopy. *Philos Mag A* 1999, **79**: 847–858.

[175] Burkovsky RG, Bronwald I, Andronikova D, *et al*. Triggered incommensurate transition in $PbHfO_3$. *Phys Rev B* 2019, **100**: 014107.

[176] Chao W, Yang T, Li Y. Achieving high energy efficiency and energy density in $PbHfO_3$-based antiferroelectric ceramics. *J Mater Chem C* 2020, **8**: 17016–17024.

[177] Huang XX, Zhang TF, Wang W, *et al*. Tailoring energy-storage performance in antiferroelectric $PbHfO_3$ thin films. *Mater Des* 2021, **204**: 109666.

[178] Xu B, Moses P, Pai NG, *et al*. Charge release of lanthanum-doped lead zirconate titanate stannate antiferroelectric thin films. *Appl Phys Lett* 1998, **72**: 593–595.

[179] Sharifzadeh Mirshekarloo M, Yao K, Sritharan T. Large strain and high energy storage density in orthorhombic perovskite $(Pb_{0.97}La_{0.02})(Zr_{1-x-y}Sn_xTi_y)O_3$ antiferroelectric thin films. *Appl Phys Lett* 2010, **97**: 142902.

[180] Zhang AH, Wang W, Li QJ, *et al*. Internal-strain release and remarkably enhanced energy storage performance in PLZT–$SrTiO_3$ multilayered films. *Appl Phys Lett* 2020, **117**: 252901.

[181] Dan Y, Xu H, Zou K, *et al*. Energy storage characteristics of $(Pb,La)(Zr,Sn,Ti)O_3$ antiferroelectric ceramics with high Sn content. *Appl Phys Lett* 2018, **113**: 063902.

[182] Liu P, Fan B, Yang G, *et al*. High energy density at high temperature in PLZST antiferroelectric ceramics. *J Mater Chem C* 2019, **7**: 4587–4594.

[183] Xu B, Ye Y, Cross L. Dielectric properties and field-induced phase switching of lead zirconate titanate stannate antiferroelectric thick films on silicon substrates. *J Appl Phys* 2000, **87**: 2507–2515.

[184] Markowski K, Park SE, Yoshikawa S, *et al*. Effect of compositional variations in the lead lanthanum zirconate stannate titanate system on electrical properties. *J Am Ceram Soc* 1996, **79**: 3297–3304.

[185] Zheng Q, Yang T, Wei K, *et al*. Effect of Sn:Ti variations on electric filed induced AFE–FE phase transition in PLZST antiferroelectric ceramics. *Ceram Int* 2012, **38**: S9–S12.

[186] Liu Z, Bai Y, Chen X, *et al*. Linear composition-dependent phase transition behavior and energy storage performance of tetragonal PLZST antiferroelectric ceramics. *J Alloys Compd* 2017, **691**: 721–725.

[187] Zhang L, Jiang S, Fan B, *et al*. Enhanced energy storage performance in $(Pb_{0.858}Ba_{0.1}La_{0.02}Y_{0.008})(Zr_{0.65}Sn_{0.3}Ti_{0.05})O_3$–$(Pb_{0.97}La_{0.02})(Zr_{0.9}Sn_{0.05}Ti_{0.05})O_3$ anti-ferroelectric composite ceramics by Spark Plasma Sintering. *J Alloys Compd* 2015, **622**: 162–165.

[188] Zhang G, Zhu D, Zhang X, *et al*. High-energy storage performance of $(Pb_{0.87}Ba_{0.1}La_{0.02})(Zr_{0.68}Sn_{0.24}Ti_{0.08})O_3$ antiferroelectric ceramics fabricated by the hot-press sintering method. *J Am Ceram Soc* 2015, **98**: 1175–1181.

[189] Zhang G, Liu S, Yu Y, *et al*. Microstructure and electrical properties of $(Pb_{0.87}Ba_{0.1}La_{0.02})(Zr_{0.68}Sn_{0.24}Ti_{0.08})O_3$ anti-ferroelectric ceramics fabricated by the hot-press sintering method. *J Eur Ceram Soc* 2013, **33**: 113–121.

[190] Bian F, Yan S, Xu C, *et al*. Enhanced breakdown strength and energy density of antiferroelectric $Pb,La(Zr,Sn,Ti)O_3$ ceramic by forming core-shell structure. *J Eur Ceram Soc* 2018, **38**: 3170–3176.

[191] Wang H, Liu Y, Yang T, *et al*. Ultrahigh energy-storage density in antiferroelectric ceramics with field-induced multiphase transitions. *Adv Funct Mater* 2019, **29**: 1807321.

[192] Zhang Y, Liu P, Kandula KR, *et al*. Achieving excellent energy storage density of $Pb_{0.97}La_{0.02}(Zr_xSn_{0.05}Ti_{0.95-x})O_3$ ceramics by the B-site modification. *J Eur Ceram Soc* 2021, **41**: 360–367.

[193] Liu X, Li Y, Hao X. Ultra-high energy-storage density and fast discharge speed of $(Pb_{0.98-x}La_{0.02}Sr_x)(Zr_{0.9}Sn_{0.1})_{0.995}O_3$ antiferroelectric ceramics prepared via the tape-casting

method. *J Mater Chem A* 2019, **7**: 11858–11866.

[194] Gao M, Tang X, Leung CM, *et al*. Phase transition and energy storage behavior of antiferroelectric PLZT thin films epitaxially deposited on SRO buffered STO single crystal substrates. *J Am Ceram Soc* 2019, **102**: 5180–5191.

[195] Ma B, Kwon DK, Narayanan M, *et al*. Dielectric properties and energy storage capability of antiferroelectric $Pb_{0.92}La_{0.08}Zr_{0.95}Ti_{0.05}O_3$ film-on-foil capacitors. *J Mater Res* 2009, **24**: 2993–2996.

[196] Tong S, Ma B, Narayanan M, *et al*. Lead lanthanum zirconate titanate ceramic thin films for energy storage. *ACS Appl Mater Interfaces* 2013, **5**: 1474–1480.

[197] Lin Z, Chen Y, Liu Z, *et al*. Large energy storage density, low energy loss and highly stable $(Pb_{0.97}La_{0.02})(Zr_{0.66}Sn_{0.23}Ti_{0.11})O_3$ antiferroelectric thin-film capacitors. *J Eur Ceram Soc* 2018, **38**: 3177–3181.

[198] Ma B, Kwon DK, Narayanan M, *et al*. Fabrication of antiferroelectric PLZT films on metal foils. *Mater Res Bull* 2009, **44**: 11–14.

[199] Zhang MH, Fulanović L, Egert S, *et al*. Electric-field-induced antiferroelectric to ferroelectric phase transition in polycrystalline $NaNbO_3$. *Acta Mater* 2020, **200**: 127–135.

[200] Chen J, Feng D. TEM study of phases and domains in $NaNbO_3$ at room temperature. *Phys Status Solidi a* 1988, **109**: 171–185.

[201] Saito T, Adachi H, Wada T, *et al*. Pulsed-laser deposition of ferroelectric $NaNbO_3$Thin films. *Jpn J Appl Phys* 2005, **44**: 6969–6972.

[202] Koruza J, Groszewicz P, Breitzke H, *et al*. Grain-size-induced ferroelectricity in $NaNbO_3$. *Acta Mater* 2017, **126**: 77–85.

[203] Shuvaeva VA, Antipin MY, Lindeman RSV, *et al*. Crystal structure of the electric-fieldinduced ferroelectric phase of $NaNbO_3$. *Ferroelectrics* 1993, **141**: 307–311.

[204] Shimizu H, Guo H, Reyes-Lillo SE, *et al*. Lead-free antiferroelectric: xCaZrO$_3$–(1–x)NaNbO$_3$ system ($0 \le x \le 0.10$). *Dalton Trans* 2015, **44**: 10763–10772.

[205] Guo H, Shimizu H, Mizuno Y, *et al*. Strategy for stabilization of the antiferroelectric phase (Pbma) over the metastable ferroelectric phase (P21ma) to establish double loop hysteresis in lead-free (1−x)NaNbO$_3$−xSrZrO$_3$ solid solution. *J Appl Phys* 2015, **117**: 214103.

[206] Gao L, Guo H, Zhang S, *et al*. A perovskite lead-free antiferroelectric xCaHfO$_3$–(1–x) NaNbO$_3$ with induced double hysteresis loops at room temperature. *J Appl Phys* 2016, **120**: 204102.

[207] Gao L, Guo H, Zhang S, *et al*. Stabilized antiferroelectricity in xBiScO$_3$–(1−x)NaNbO$_3$ lead-free ceramics with established double hysteresis loops. *Appl Phys Lett* 2018, **112**: 092905.

[208] Zhou M, Liang R, Zhou Z, *et al*. Superior energy storage properties and excellent stability of novel $NaNbO_3$-based lead-free ceramics with A-site vacancy obtained via a Bi_2O_3 substitution strategy. *J Mater Chem A* 2018, **6**: 17896–17904.

[209] Ye J, Wang G, Zhou M, *et al*. Excellent comprehensive energy storage properties of novel lead-free $NaNbO_3$-based ceramics for dielectric capacitor applications. *J Mater Chem C* 2019, **7**: 5639–5645.

[210] Dong X, Li X, Chen X, *et al*. High energy storage density and power density achieved simultaneously in $NaNbO_3$-based lead-free ceramics via antiferroelectricity enhancement. *J Materiomics* 2021, **7**: 629–639.

[211] Fujii I, Shimasaki T, Nobe T, *et al*. Effects of $SrTiO_3$ substrate orientations on crystal and domain structures and electric properties of $NaNbO_3$–$SrZrO_3$ films. *Jpn J Appl Phys* 2018, **57**: 11UF13.

[212] Beppu K, Shimasaki T, Fujii I, *et al*. Energy storage properties of antiferroelectric $0.92NaNbO_3$–$0.08SrZrO_3$ film on (001)$SrTiO_3$ substrate. *Phys Lett A* 2020, **384**: 126690.

[213] Luo B, Dong H, Wang D, *et al*. Large recoverable energy density with excellent thermal stability in Mn-modified $NaNbO_3$–$CaZrO_3$ lead-free thin films. *J Am Ceram Soc* 2018, **101**: 3460–3467.

[214] Kania A, Kwapulinski J. $Ag_{1-x}Na_xNbO_3$ (ANN) solid solutions: From disordered antiferroelectric $AgNbO_3$ to normal antiferroelectric $NaNbO_3$. *J Phys*: *Condens Matter* 1999, **11**: 8933–8946.

[215] Wang D, Kako T, Ye J. New series of solid-solution semiconductors $(AgNbO_3)_{1-x}(SrTiO_3)_x$ with modulated band structure and enhanced visible-light photocatalytic activity. *J Phys Chem C* 2009, **113**: 3785–3792.

[216] Fu D, Endo M, Taniguchi H, *et al*. $AgNbO_3$: A lead-free material with large polarization and electromechanical response. *Appl Phys Lett* 2007, **90**: 252907.

[217] Tian Y, Jin L, Zhang H, *et al*. High energy density in silver niobate ceramics. *J Mater Chem A* 2016, **4**: 17279–17287.

[218] Zhao L, Liu Q, Gao J, *et al*. Lead-free antiferroelectric silver niobate tantalate with high energy storage performance. *Adv Mater* 2017, **29**: 1701824.

[219] Luo N, Han K, Cabral MJ, *et al*. Constructing phase boundary in $AgNbO_3$ antiferroelectrics: Pathway simultaneously achieving high energy density and efficiency. *Nat Commun* 2020, **11**: 4824.

[220] Yan Z, Zhang D, Zhou X, *et al*. Silver niobate based lead-free ceramics with high energy storage density. *J Mater Chem A* 2019, **7**: 10702–10711.

[221] Luo N, Han K, Zhuo F, *et al*. Aliovalent A-site engineered $AgNbO_3$ lead-free antiferroelectric ceramics toward superior energy storage density. *J Mater Chem A* 2019, **7**: 14118–14128.

[222] Lu Z, Bao W, Wang G, *et al*. Mechanism of enhanced energy storage density in $AgNbO_3$-based lead-free antiferroelectrics. *Nano Energy* 2021, **79**: 105423.

[223] Zhao L, Gao J, Liu Q, *et al*. Silver niobate lead-free antiferroelectric ceramics: Enhancing energy storage density by B-site doping. *ACS Appl Mater Interfaces* 2018, **10**: 819–826.

[224] Tian Y, Jin L, Zhang H, *et al*. Phase transitions in bismuth-modified silver niobate ceramics for high power energy storage. *J Mater Chem A* 2017, **5**: 17525–17531.

[225] Luo N, Han K, Zhuo F, *et al*. Design for high energy storage density and temperature-insensitive lead-free antiferroelectric ceramics. *J Mater Chem C* 2019, **7**: 4999–5008.

[226] Gao J, Zhang Y, Zhao L, *et al*. Enhanced antiferroelectric phase stability in La-doped $AgNbO_3$: Perspectives from the microstructure to energy storage properties. *J Mater Chem A* 2019, **7**: 2225–2232.

[227] Han K, Luo N, Mao S, *et al*. Realizing high low-electric-field energy storage performance in $AgNbO_3$ ceramics by introducing relaxor behaviour. *J Materiomics* 2019, **5**: 597–605.

[228] Wang J, Wan X, Rao Y, *et al*. Hydrothermal synthesized $AgNbO_3$ powders: Leading to greatly improved electric breakdown strength in ceramics. *J Eur Ceram Soc* 2020, **40**: 5589–5596.